Manuscript Details

Manuscript number	*LUMIN_2017_2018*
Title	*Cubic and rhombohedral Ba4Lu3F17:Er3+ in transparent glass ceramics: crystallization and upconversion luminescence*
Article type	*Research Paper*

Abstract

Novel Er3+ doped glass ceramics containing Ba4Lu3F17 nanocrystals were successfully prepared by heat treatment of melt-quenched glasses. Highly efficient upconversion luminescence was detected under near-infrared excitation and it was at least two orders of magnitude higher than that in the precursor glass. The activator content in the crystalline phase was estimated using polycrystalline Ba4Lu3F17 with different Er3+ content as the reference and it was found to be higher than in similar glass ceramics. The structure and thermal analysis of the glass ceramics revealed the formation of cubic and rhombohedrally distorted cubic modifications of Ba4Lu3F17. Phase transition between the two modifications was studied using site selective spectroscopy of Er3+ as a structural probe. Unusually efficient incorporation of Er3+ ions in the Ba4Lu3F17 nanocrystals combined with the low phonon energy of the fluoride crystals make this material a desirable host for upconversion luminescence.

Keywords	*upconversion; luminescence; Ba4Lu3F17; site-selective spectroscopy; glass ceramics*
Manuscript category	*Up/down conversion, quantum cutting + energy transfer (inorganic ions)*

Corresponding Author	*Guna Krieke*
Corresponding Author's Institution	*Institute of Solid State Physics*
Order of Authors	*Guna Krieke, Anatolijs Sarakovskis, Maris Springis*

Suggested reviewers	*Pavel Fedorov, Araceli de Pablos-Martín, Daqin Chen*

Submission Files Included in this PDF

File Name [File Type]

Cover letter.docx [Cover Letter]

Ba4Lu3F17-6-bezMendeley1.doc [Manuscript File]

Fig-1-DTA.tif [Figure]

Fig-2-XRD.tif [Figure]

Fig-3-XRD.tif [Figure]

BLuF-SEM.eps [Figure]

Fig-5-UCL.tif [Figure]

Fig-6-UCL.tif [Figure]

Fig-7-photo.jpg [Figure]

Fig-8-power.tif [Figure]

Fig-9-content.tif [Figure]

Fig-10-en-levels.tif [Figure]

Fig-11-PL.tif [Figure]

Fig-12-PLE.tif [Figure]

Fig-13-PLE.tif [Figure]

Fig-14-PLE.tif [Figure]

To view all the submission files, including those not included in the PDF, click on the manuscript title on your EVISE Homepage, then click 'Download zip file'.

COVER LETTER

Dear Editor,

Please, accept the manuscript "**Cubic and rhombohedral $Ba_4Lu_3F_{17}$:Er^{3+} in transparent glass ceramics: crystallization and upconversion luminescence**" for publication in the Journal of Luminescence.

The article is original, has been written by the stated authors who are all aware of its content and approve its submission, has not been published previously, it is not under consideration for publication elsewhere, no conflict of interest exists.

If accepted, the article will not be published elsewhere in the same form, in any language, without the written consent of the publisher. The submission of this manuscript to your journal has been accepted the approval from all of other co-authors.

Cubic and rhombohedral $Ba_4Lu_3F_{17}:Er^{3+}$ in transparent glass ceramics: crystallization and upconversion luminescence

Guna Krieke*, Anatolijs Sarakovskis, Maris Springis

Institute of Solid State Physics, University of Latvia, 8 Kengaraga str., LV-1063, Riga, Latvia.

*Corresponding author, e-mail: guna.krieke@cfi.lu.lv

Abstract

Novel Er^{3+} doped glass ceramics containing $Ba_4Lu_3F_{17}$ nanocrystals were successfully prepared by heat treatment of melt-quenched glasses.

Highly efficient upconversion luminescence was detected under near-infrared excitation and it was at least two orders of magnitude higher than that in the precursor glass. The activator content in the crystalline phase was estimated using polycrystalline $Ba_4Lu_3F_{17}$ with different Er^{3+} content as the reference and it was found to be higher than in similar glass ceramics.

The structure and thermal analysis of the glass ceramics revealed the formation of cubic and rhombohedrally distorted cubic modifications of $Ba_4Lu_3F_{17}$. Phase transition between the two modifications was studied using site selective spectroscopy of Er^{3+} as a structural probe.

Unusually efficient incorporation of Er^{3+} ions in the $Ba_4Lu_3F_{17}$ nanocrystals combined with the low phonon energy of the fluoride crystals make this material a desirable host for upconversion luminescence.

KEYWORDS: upconversion, luminescence**,** $Ba_4Lu_3F_{17}$, site-selective spectroscopy, glass ceramics

Introduction

Transparent oxyfluoride glass ceramics have been widely investigated for promising applications in photonics such as in solid state lasers [1], optical thermometry [2,3], X-ray imaging [4,5], non-linear optics [6], holographic recording [7], optical cooling [8] and light conversion devices [9,10]. These composites contain fluoride nanocrystals dispersed in glass matrix and combine the good mechanical and chemical stability of oxides with the excellent optical properties of fluorides [11,12].

Rare earth (RE) doped oxyfluoride glass ceramics are found to be suitable for upconversion luminescence (UCL) – an anti-Stokes process in which photons with lower energy are converted to ones with higher energy [13]. The highest UCL quantum yield has been detected in Er^{3+} doped materials, which are extensively investigated for near-infrared to visible UCL [14]. It is known, that an efficient UCL process requires suitable host with good Er^{3+} solubility, low phonon energy and low

local symmetry of activator ions. Among others, fluorite type (face centred cubic) BaF_2 fulfils all the requirements. However, despite the excellent solubility of activators, Er^{3+} ions tend to form clusters in the BaF_2 lattice, leading to increased rate of non-radiative cross-relaxations and reduction of the UCL efficiency [15]. This effect is reviewed in details elsewhere [16]. The clustering of the activator ions can be prevented by the introduction of other RE ions such as La^{3+}, Gd^{3+}, Y^{3+} or Lu^{3+} in the BaF_2 lattice, that would replace Er^{3+} ions in the clusters, therefore increasing the average distances between activators and diminish the rate of the cross-relaxation processes.

Wide regions of solid solutions with fluorite structure has been detected in all BaF_2-REF_3 binary systems [17,18]. In addition, two distorted fluorite phases are known: $Ba_4RE_3F_{17}$ (RE=Sm-Lu) with rhombohedral distortion and high temperature modification Ba_2REF_7 (RE=Dy-Lu) with tetragonally distorted fluorite structure [18,19]. In oxyfluoride glass ceramics the formation of several fluorite type phases such as Ba_2LaF_7 [20], $BaGdF_5$ [21], $BaYF_5$ [22], $BaYbF_5$ [23], $BaLuF_5$ [24] and rhobohedrally distorted fluorite phases $Ba_4Gd_3F_{17}$ [25], $Ba_4Y_3F_{17}$ [26], $Ba_4Yb_3F_{17}$ [27] have been reported.

In oxyfluoride glasses the high field strength cations such as RE ions are mainly located in the fluoride environment, enabling the incorporation of rare earth activators in the fluoride nanocrystals [28]. Nevertheless, in systems containing several RE ions different efficiencies of the incorporation of RE ions in crystalline phases can be expected. Comprehensive investigation of experimentally determined liquid–liquid distribution coefficients of RE ions in fluoride containing silicate melts revealed that all RE ions exhibit high tendency to incorporate in fluoride-rich phase [29]. However, this tendency gradually declines with the decrease of ionic radii of trivalent RE ion following the trend La>Lu. This effect has been also reported in oxyfluoride glass ceramics [30], suggesting that the ionic radii of the activator should be larger than that of RE containing host for efficient incorporation of activator ions in the fluoride-rich phase. For example, in glass ceramics containing Eu^{3+} doped LaF_3, the activator ions were found to be evenly distributed in nanocrystals and glass matrix [31], but in Tm^{3+} doped LaF_3 the activator content was estimated to be only 17-20% [32].

We have recently developed new glass ceramics containing $Ba_4RE_3F_{17}$ (RE=Gd, Y and Yb) [25–27]. For Er^{3+} doped materials, hosts containing Lu^{3+} should ensure efficient incorporation of activation ions in the crystalline phase.

This research is devoted to the investigation of novel Er^{3+} doped glass ceramics containing $Ba_4Lu_3F_{17}$ nanocrystals. The Er^{3+} is used both as activator for UCL and probe for the analysis of erbium content in the nanocrystals and changes in the local environment during the growth of the crystalline phase.

Materials and methods

Precursor glasses with nominal composition of $15Na_2O$-3NaF-$6BaF_2$-$xErF_3$-(7-x)LuF_3-$6Al_2O_3$-$63SiO_2$ (x=0.1-3) in mol% were prepared from high purity raw

materials. The batches of 9 g were melted in covered corundum crucibles at 1500^{0}C for 30 min and afterwards casted in stainless steel mould. The glass ceramics were obtained after isothermal heat treatment of the precursor glasses at 550-700^{0}C for 2 h.

Polycrystalline cubic $Ba_4Lu_3F_{17}$ doped with 1% ErF_3 was prepared using co-precipitation. Mixture of $LuCl_3{\cdot}xH_2O$ and $ErCl_3{\cdot}xH_2O$ was prepared by dissolving 1.485 mmol Lu_2O_3 and 0.015 mmol Er_2O_3 in concentrated HCl. The excess HCl and water were removed by evaporation. 4 mmol $BaCl_2{\cdot}2H_2O$ was dissolved in 10 ml deionized water and added to the chlorides. The resulting solution was stirred for 15 min to ensure complete dissolution. 10 ml 37.5 mmol NH_4F was dissolved in deionized water and added to the solution causing the precipitation of $Ba_4RE_3F_{17}$. The suspension was stirred for 3 h. Afterwards the product was collected by filtration and dried in air.

Polycrystalline rhombohedral $Ba_4Lu_3F_{17}$ doped with 1, 2, 5, 10, 20, 40, 60 and 100% Er^{3+} was prepared using hydrothermal synthesis adapted from [27]. The as-prepared samples were annealed at 150^{0}C in He/F_2 flow for 1 h to remove adsorbed water and OH^- impurities and afterwards heat treated at 650^{0}C in Ar flow for 1 h to improve the crystallinity of the rhombohedral $Ba_4RE_3F_{17}$.

The differential thermal analysis (DTA) was performed using differential thermal analyser (Shimadzu Corp. DTG-60) at a heating rate of 10 K/min and using Al_2O_3 as a reference. The characteristic temperatures were detected with ±1°C precision.

X-ray diffraction data was obtained by PANalytical X'Pert Pro diffractometer using Cu K_α tube operated at 45 kV and 40 mA. The Rietveld analysis was performed using Profex software [30].

The microstructure of the glass ceramics was analysed by scanning electron microscopy (SEM) using Tescan Lyra operated at 15 kV. Uncoated, fractured surfaces of the glass and glass ceramics were analysed.

Luminescence was excited by a wavelength tuneable pulsed solid state laser Ekspla NT342/3UV and temperature controlled continuous wave laser diode (λ_{em}= 975 nm, variable radiant power up to 1 W). The emission signal was detected by Andor DU-401-BV CCD camera coupled to Andor SR-303i-B spectrometer. Luminescence decay was measured using a photomultiplier tube and digital oscilloscope Tektronix TDS 684A. Low temperature measurements were performed using Advanced Research Systems DE202 N cold finger type He cryostat.

Results and discussion

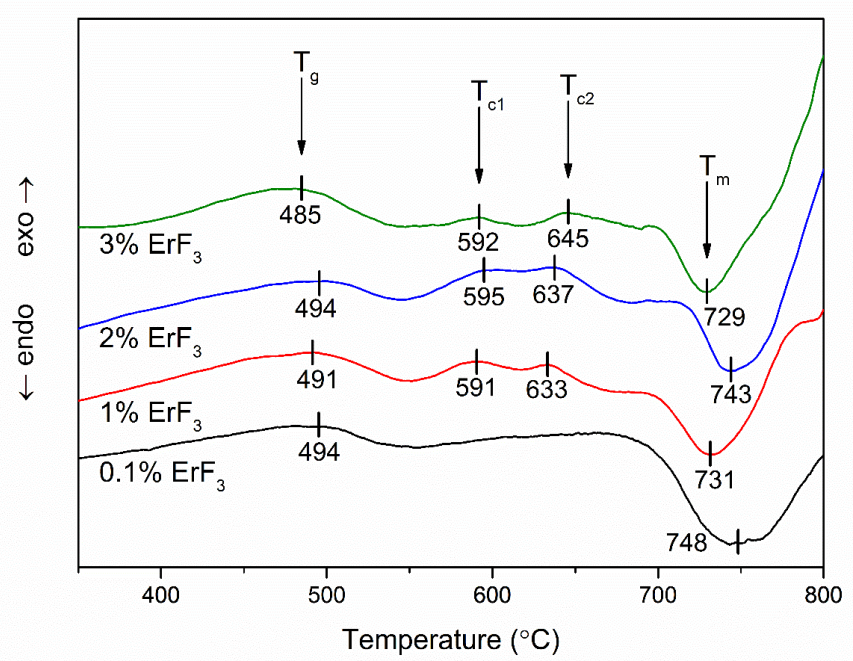

Fig. 1. DTA curves of precursor glasses doped with 0.1-3% ErF_3.

The DTA curves of the precursor glasses are shown in Fig. 1. The glass transition temperature (T_g) is located at 491±4°C and varies slightly for the glass ceramics with different ErF_3 content, possibly due to deviations in the fluorine content of the precursor glasses. For the glass ceramics with 0.1% ErF_3 no intense exothermic effects associated with the crystallization of the fluoride phases were detected. The increase of the ErF_3 content promoted the crystallization, indicated by two distinct exothermic effects T_{c1} and T_{c2} located at approximately 593±2°C and 638±6°C associated with the crystallization of the fluoride phases. Slight increase of T_{c2} with the ErF_3 content suggests that the replacement of LuF_3 with ErF_3 alters the chemical composition of the fluorite phase due to efficient incorporation of Er^{3+} ions in the crystalline phase. T_{c2} is followed by an endothermic effect T_m associated with the melting of the precursor glasses.

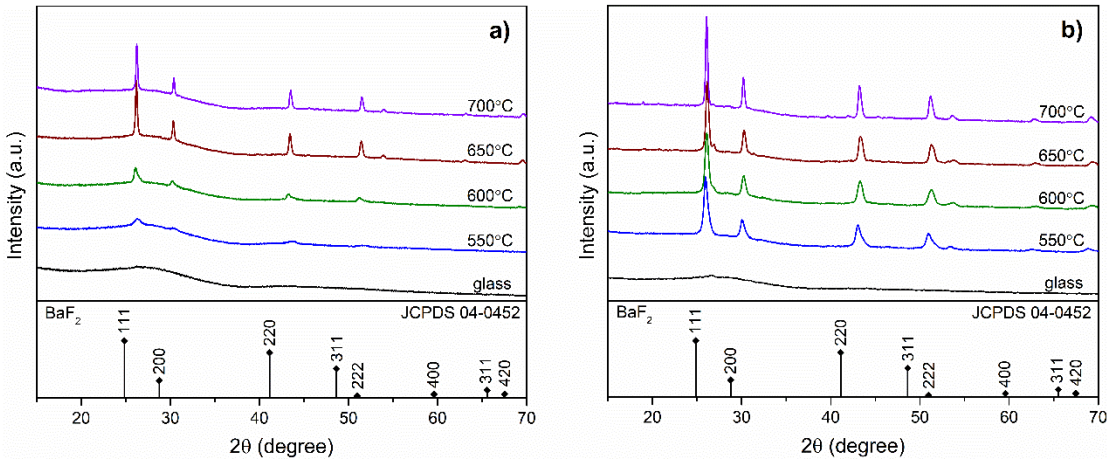

Fig. 2. XRD patterns of the precursor glass and glass ceramics with a) 0.1% ErF_3 and b) 1.0% ErF_3 heat treated at different temperatures for 2 h.

The XRD patterns of the precursor glasses and glass ceramics heat treated at 550-700°C for 2 h, doped with 0.1% and 1% ErF_3 are represented in Fig. 2. No intense diffraction peaks were detected in the investigated glasses indicating the amorphous nature of the precursors. Despite the absence of intense exothermic effects associated with the crystallization of fluoride phases in the glass ceramics with 0.1% ErF_3 (see Fig. 1), XRD analysis of the heat treated glass samples shows presence of the fluorite type phase similar to cubic BaF_2. The intensity of the diffraction peaks was considerably higher in the glass ceramics doped with 1% ErF_3 (see Fig. 2 b) suggesting that the replacement of LuF_3 with ErF_3 improves the crystallization and it is in a good agreement with the DTA data shown in Fig.1. The lattice parameter of the crystalline phase a=5.886±0.003 Å for glass ceramics heat treated at 700°C for 2 h is considerably smaller than BaF_2 (a=6.200 Å), suggesting the formation of BaF_2-REF_3 compound. The increase of the temperature of the heat treatment resulted in the enhancement of the intensity and narrowing of the XRD peaks due to growth of the nanocrystals. In the glass ceramics doped with 1% ErF_3, two distinct exothermic effects associated with the crystallization were detected by DTA, however, no considerable changes in the phase composition could be detected by XRD. Such processes have been observed in similar glass ceramics and ascribed to order-disorder phase transitions

[25,27]. Only one ordered phase with rhombohedrally distorted fluorite structure and general composition of $Ba_4Lu_3F_{17}$ has been observed in BaF_2-LuF_3 binary system [33]. Besides the rhombohedral phase another modification – cubic $Ba_4RE_3F_{17}$ with fluorite structure can be obtained in metastable systems [34]. The formation of two modifications with fluorite and distorted fluorite structure agree well with both DTA and XRD data.

The rhombohedral phase can be distinguished from the cubic phase by superstructure peaks characteristic to rhombohedral distortion in the fluorite lattice [25]. To detect such small changes in the crystalline lattice, high-resolution XRD was analysed.

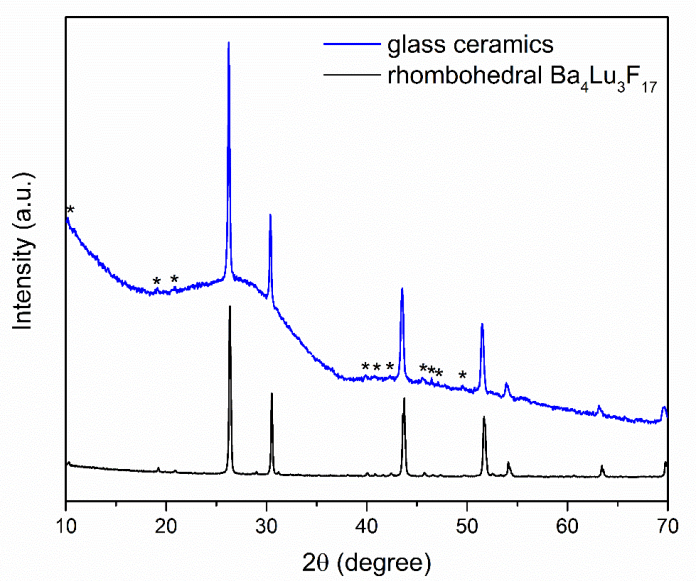

Fig. 3. XRD patterns of the glass ceramics with 0.1% ErF_3 heat treated at 700°C for 2 h and polycrystalline rhombohedral $Ba_4Lu_3F_{17}$ (superstructure peaks are marked with *)

Weak superstructure peaks marked with * are observed in the glass ceramics heat treated at 700°C for 2 h that are in good agreement with polycrystalline rhombohedral $Ba_4Lu_3F_{17}$ (see Fig. 3). The results indicate that rhombohedral $Ba_4Lu_3F_{17}$ is indeed present in these materials at high temperatures. Unfortunately, a phase transition from fluorite to rhombohedrally distorted fluorite structure cannot be detected in the investigated glass ceramics due to weak superstructure peaks of the rhombohedral phase and relatively small size of the nanocrystals that prevents the detection of the rhombohedral phase in the glass ceramics heat treated at 550-650° C.

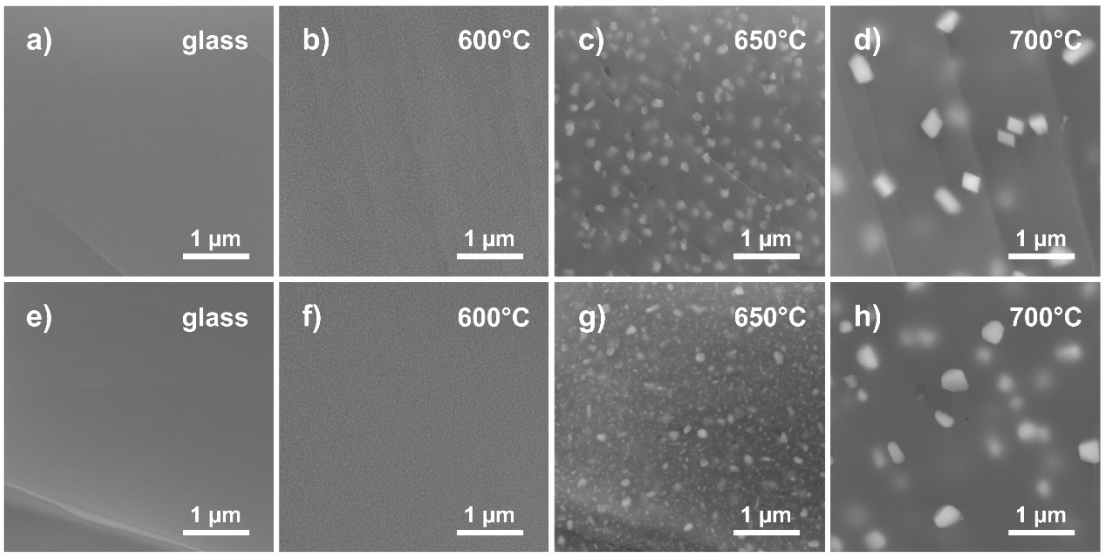

Fig. 4. SEM micrographs of glass and glass ceramics heat treated at 600-700°C 2 h doped with 0.1 % ErF_3 (a-d) and 1% ErF_3 (e-h).

The microstructure of the precursor glass and glass ceramics are shown in Fig. 4. No micro-scale heterogeneities were detected in the precursor glasses. After the heat treatment at 600°C for 2 h, bright spots could be detected corresponding to the regions

enriched in heavy element ions (Ba^{2+}, Er^{3+}, Lu^{3+}) homogeneously distributed in the glass matrix containing lighter element ions (such as Si^{4+}, Al^{3+} and Na^{+}). Further increase of the heat treatment temperature promoted the growth of the nanocrystals. The size of the nanocrystals increased after the heat treatment at higher temperature, however the number of the crystals was considerably reduced. This effect can be attributed to the decrease of nucleation rate at higher temperatures or Ostwald's ripening shown in similar oxyfluoride glass ceramics [25]. The nanocrystals in the glass ceramics doped with 0.1% ErF_3 resemble well defined rhombohedral prisms and are found to be with narrower size distribution than in glass ceramics with higher doping content, nevertheless, the microstructure was similar for all the glass ceramics.

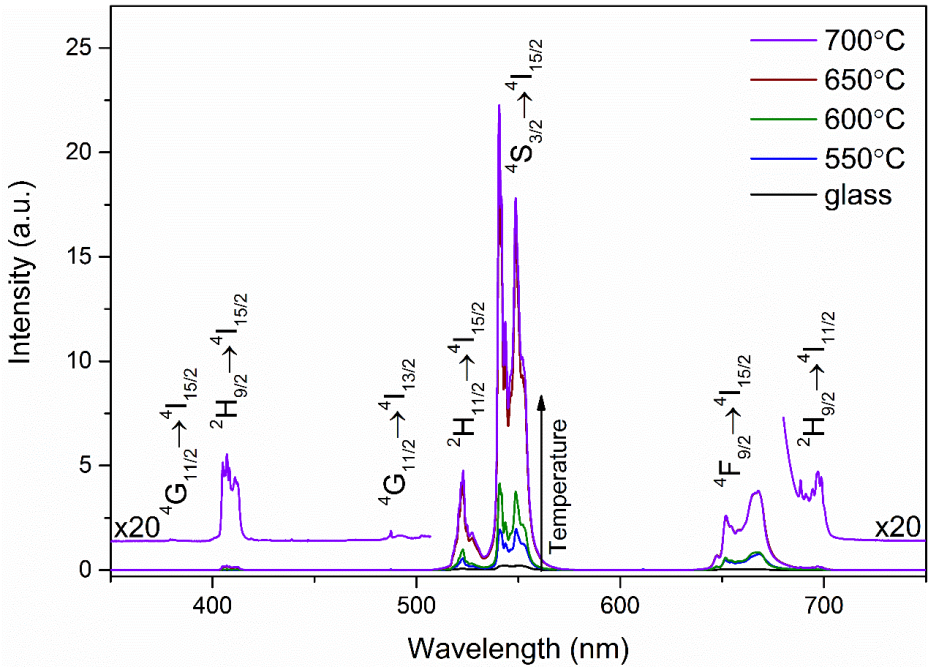

Fig. 5. UCL spectra under 975 nm excitation of the precursor glass and glass ceramics doped with 0.1% ErF_3 heat treated at 550-700^{0}C for 2 h

The UCL spectra of the precursor glass and glass ceramics doped with 0.1% ErF_3 are shown in Fig. 5. In the precursor glass low intensity UCL can be detected, however, it is significantly increased after the heat treatment of the precursor. Narrow and intense UCL peaks can be detected in the glass ceramics indicating the incorporation of Er^{3+} ions in the crystalline environment. The most intense UCL bands were assigned to $^2H_{11/2}\rightarrow{}^4I_{15/2}$, $^4S_{3/2}\rightarrow{}^4I_{15/2}$ and $^4F_{9/2}\rightarrow{}^4I_{15/2}$ transitions of Er^{3+} ions resulting in the green and red emission. In addition, several weaker bands associated with the transitions from $^4G_{11/2}$ and $^2H_{9/2}$ energy levels to the lower lying states could be detected. The UCL intensity of the glass ceramics heat treated at 650-700°C was approximately 5-10 times higher than in glass ceramics heat treated at 550-600°C and at least two orders of magnitude higher than that of the precursor glass. The enhancement of the UCL efficiency in the glass ceramics can be explained by the incorporation of Er^{3+} ions in the low-phonon environment of fluoride crystals where the rate of the non-radiative transitions is smaller. In addition, there is considerable enhancement of the UCL intensity when the temperature of the heat treatment is increased. Several factors can contribute to this effect, such as the reduction of the surface area during the

growth of the crystals or the changes in the local environment of the Er^{3+} ions due to phase transition from metastable to ordered phase. The latter effect will be analysed in details further in the text.

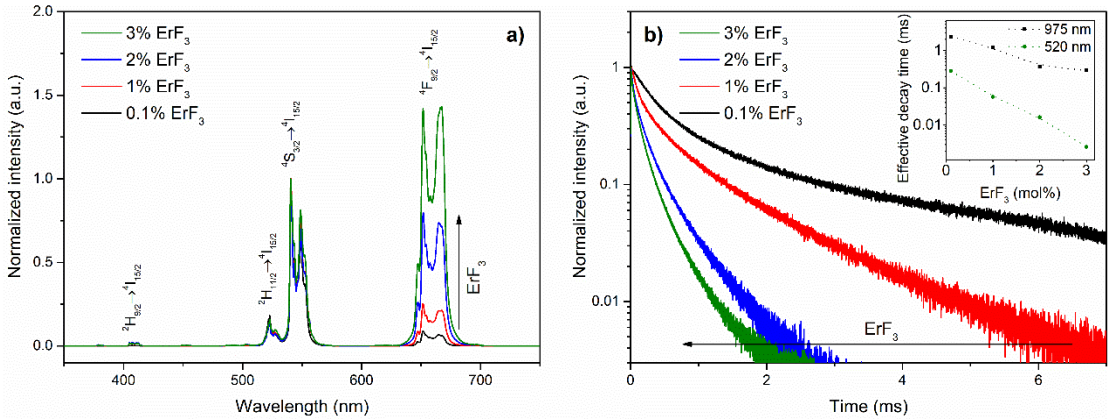

Fig. 6. a) UCL spectra of glass ceramics doped with 0.1-3% ErF_3 heat treated at 650°C for 2 h under 975 nm excitation and b) Luminescence decay of green emission under 975 nm excitation. Inset: effective lifetime of the green emission excited at 975 nm and 520 nm.

The comparison of the UCL spectra of the glass ceramics doped with 0.1-3% ErF_3 at 650°C for 2 h are shown in Fig. 6 a). The increase of the Er^{3+} content in the precursor glass drastically change the relative intensity ratio of the green and red emission bands of the glass ceramics; the ratio is considerably higher than in similar $Ba_4RE_3F_{17}$ containing glass ceramic systems reported previously and it is attributed to enhanced rate of cross-relaxation processes between erbium ions [25,26]. The photographs of glass ceramic doped with 0.1-3% ErF_3 are shown in Fig. 7.

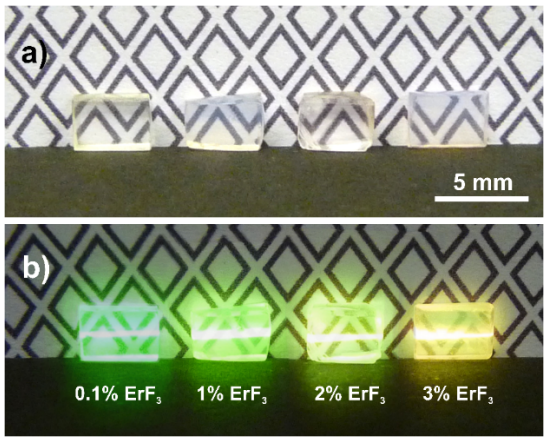

Fig. 7. Photographs of glass ceramics doped with 0.1-3 mol% ErF_3 heat treated at 650^0C for 2 h: a) as prepared, b) excited with 975 nm continuous wave laser.

The higher rate of the cross-relaxation processes implies both the appearance of additional pathways to populate the red emitting state and the reduction of the effective decay time of the green emitting state. The effective decay time of the green emission observed in the UCL process is considerably longer in comparison to that

obtained under direct excitation (see inset of Fig. 6 b) indicating that even for the glass ceramics with the lowest Er^{3+} content energy transfer is the dominant UCL mechanism in the investigated materials.

The UCL mechanisms are often investigated by the dependence of the UCL intensity I on pump power P. In the case of small upconversion rates, UCL intensity I is proportional to n-th power of P. The value of n is the number of photons required to populate the emitting states [35].

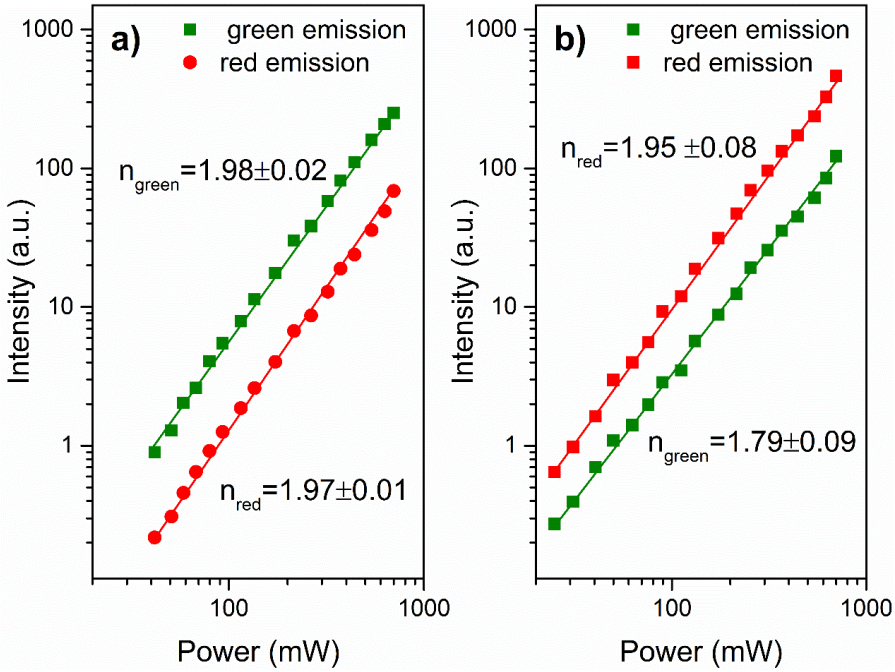

Fig. 8. Power dependence of the green ($^4S_{3/2} \rightarrow {}^4I_{15/2}$) and red ($^4F_{9/2} \rightarrow {}^4I_{15/2}$) UCL emission in the glass ceramics doped with a) 0.1% and b) 3% ErF_3 under 975 nm excitation.

The power dependence of the dominant UCL band intensity is shown in Fig. 8. For the glass ceramics with low ErF_3 content (see Fig. 8 a) the slopes of log-log plots for the green and red emission are approximately the same (n_{green}=1.98±0.02 and n_{red}=1.97±0.01). The values are close to n=2 suggesting that two photon UCL is the dominant mechanism for the population of these emitting states. As expected, due to the improved energy transfer efficiency [35], for the glass ceramics with high Er^{3+} content (3% ErF_3) the slopes for the green emission is lower n_{green}=1.79±0.09 (see Fig. 8 b). However, the slope of the red emission n_{red}=1.95±0.08 is quite high, suggesting that both two and three photon UCL contribute to the population of the red emitting state.

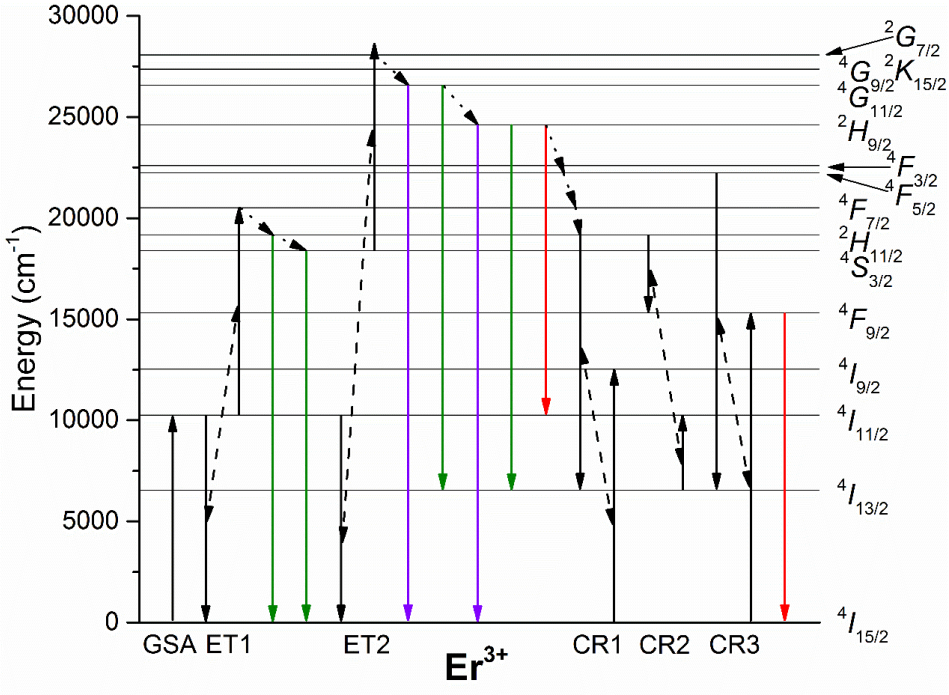

Fig. 9. Partial energy level diagram of Er^{3+} ions and dominant UCL mechanisms in the glass ceramics.

The dominant UCL processes of glass ceramics heat treated at 650°C for 2 h are represented in Fig. 9. In the investigated materials Er^{3+} ions are excited from $^4I_{15/2}$ to $^4I_{11/2}$ by ground state absorption (GSA). In the investigated glass ceramics energy transfer is the dominant UCL process for the population of the emitting states (see Inset of Fig. 6 b), therefore Er^{3+} ions are further excited to $^4F_{7/2}$ mainly by energy transfer between neighbouring Er^{3+} ions: $^4I_{11/2}$;$^4I_{11/2}\rightarrow{}^4F_{7/2}$;$^4I_{15/2}$ (ET1). The rapid non-radiative relaxation from $^4F_{7/2}$ populates $^2H_{11/2}$ and $^4S_{3/2}$, resulting in the generation of the green luminescence. The relatively long lifetime of $^4S_{3/2}$ and $^4I_{11/2}$ enables energy transfer $^2H_{11/2}$,$^4S_{3/2}$;$^4I_{11/2}\rightarrow{}^2G_{7/2}$;$^4I_{15/2}$ (ET2). Non-radiative transitions from $^2G_{7/2}$ populate the levels, responsible for a series of transitions from $^4G_{11/2}$ and $^2H_{9/2}$ to $^4I_{15/2}$, $^4I_{13/2}$ and $^4I_{11/2}$ observed in the ultraviolet, violet, green and red spectral region. As for the red emission, the non-radiative decay from $^4S_{3/2}$ to $^4F_{9/2}$ is not expected to be efficient in fluorides therefore the population of this state is realised by cross-relaxation. The dominant cross-relaxations processes are expected to be two subsequent processes CR1 and CR2 ($^2H_{11/2}$,$^4S_{3/2}$;$^4I_{15/2}\rightarrow{}^4I_{13/2}$;$^4I_{9/2}$) followed by ($^2H_{11/2}$,$^4S_{3/2}$;$^4I_{13/2}\rightarrow{}^4F_{9/2}$;$^4I_{11/2}$) corresponding to two photon UCL. However, according to the power dependence of UCL intensity of red emission in glass ceramics with high Er^{3+} content, contribution from three photon UCL resulting in CR3 ($^4F_{3/2}$,$^4F_{5/2}$;$^4I_{15/2}\rightarrow{}^4I_{13/2}$;$^4F_{9/2}$) have to be considered.

As mentioned previously, in the investigated glass ceramics efficient incorporation of Er^{3+} ions in the nanocrystals is expected. Due to the inert nature of the glass matrix and small size of nanocrystals, the analysis of the chemical composition of the crystalline phase is difficult. In this research the Er^{3+} content in the rhombohedral $Ba_4Lu_3F_{17}$ nanocrystals was estimated by the comparison of the effective decay time of the green emission and red/green emission ratio of the glass ceramics with the

corresponding parameters for the polycrystalline rhombohedral $Ba_4Lu_3F_{17}$ doped with 1-100% ErF_3. To reduce the effect of luminescence quenching on the surface of the nanocrystals, glass ceramics with the largest crystal size (heat treated at 700°C for 2 h) were used. Due to the efficiency of the cross-relaxation process CR3 (see Fig. 9) that results in the population of the red emitting state, the glass ceramics and polycrystalline ceramics were excited at 445 nm.

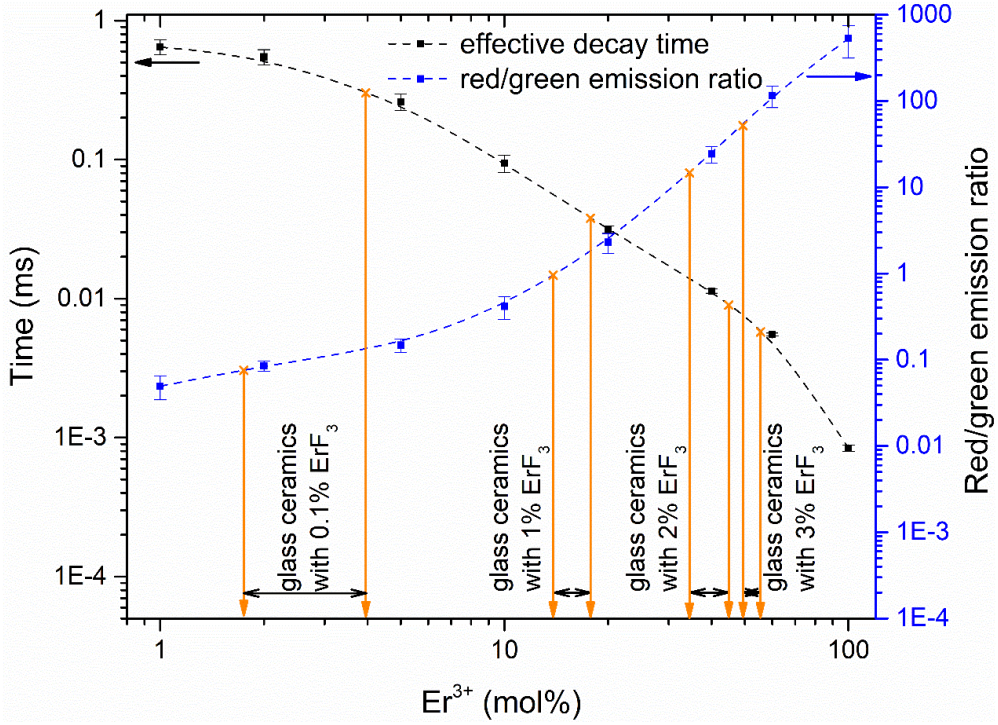

Fig. 10 The effective decay time of $^4S_{3/2} \rightarrow {}^4I_{15/2}$ emission and red/green emission ratio of Er^{3+} in polycrystalline $Ba_4Lu_3F_{17}$, excited at 445 nm. x and droplines mark the values of glass ceramics heat treated at 700°C for 2 h.

The effective decay time of $^4S_{3/2} \rightarrow {}^4I_{15/2}$ emission and red/green emission ratio of Er^{3+} in polycrystalline $Ba_4Lu_3F_{17}$, excited at 445 nm shown in Fig. 10. were found to be highly dependent on the Er^{3+} content in the material. Both of these parameters were compared with the values detected in the glass ceramics marked with x in Fig. 10. Slightly different values were obtained from the comparison of effective decay time and red/green emission ration of the glass ceramics with the values detected in polycrystalline samples. Higher Er^{3+} content was estimated from the effective decay time. We assume that it was slightly overestimated due to some degree of luminescence quenching on the surface of nanocrystals. Nevertheless, quite good agreement was found for the effective decay time of $^4S_{3/2} \rightarrow {}^4I_{15/2}$ emission and red/green emission ratio.

In the oxyfluoride melts all RE ions preferably incorporate in the fluoride environment, therefore, in the glass ceramics we could expect most of RE ions incorporated in the crystalline environment. In the investigated glass ceramics deviations from the expected Er^{3+} content, assuming complete incorporation of RE ions in the crystalline environment, were detected.

Table 1

Er^{3+} content in $Ba_4Lu_3F_{17}$ nanocrystals

ErF_3 in precursor glass (mol%)	Er^{3+} content in $Ba_4Lu_3F_{17}$ nanocrystals (mol%)	
	Expected	Estimated
0.1	1.4	2.8±1.1
1	14.3	15.8±2.1
2	28.6	39.4±5.2
3	42.9	52.2±2.8

The expected and estimated Er^{3+} content in $Ba_4Lu_3F_{17}$ nanocrystals is summarized in Table 1. Considerably higher Er^{3+} content was detected in the $Ba_4Lu_3F_{17}$ nanocrystals indicating the preferential incorporation of Er^{3+} ions over Lu^{3+} in the oxyfluoride glass ceramics. This effect should apply to all RE^{3+} containing glass ceramics, therefore, the optical properties of Er^{3+} ions in $Ba_4Lu_3F_{17}$ nanocrystals were compared with $Ba_4Gd_3F_{17}$ and $Ba_4Y_3F_{17}$ nanocrystals obtained in similar oxyfluoride glass ceramics reported previously [25,26].

Due to different non-radiative relaxation rates of Er^{3+} ions in the crystalline and glassy phases, Er^{3+} in each of them can be selectively excited using time-resolved site-selective spectroscopy.

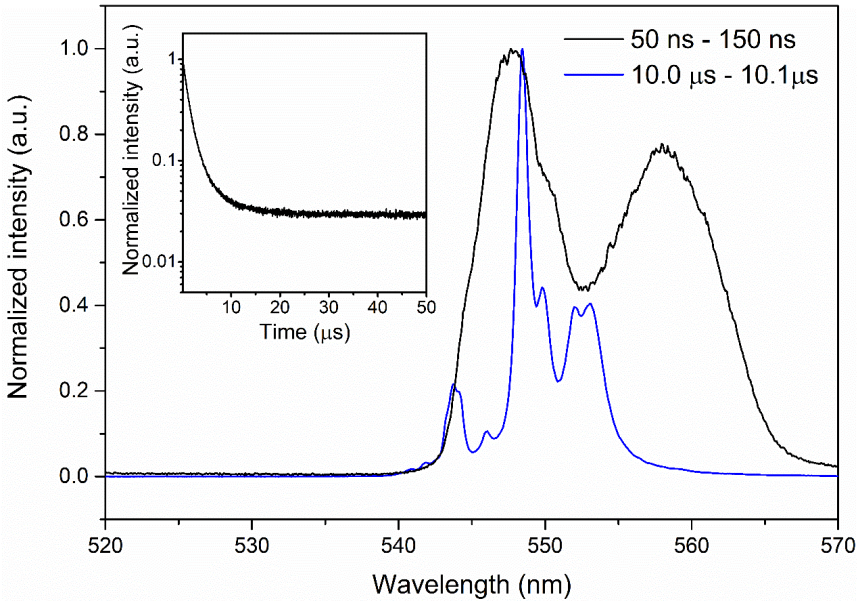

Fig. 11. Time-resolved luminescence spectra of the glass ceramics heat treated at 700°C for 2 h doped with 1% ErF_3 containing $Ba_4Lu_3F_{17}$ nanocrystals corresponding to the fast (50 ns – 150 ns) and slow (10.0 μs – 10.1 μs) components. Luminescence was excited at 489 nm, measured at 10 K. Inset: luminescence decay of Er^{3+} ions in glass ceramics heat treated at 700°C for 2 h doped with 1% ErF_3 excited at 489 nm, measured at 10 K.

In the investigated glass ceramics two parts of luminescence decay of Er^{3+} ions can be detected (see Inset of Fig. 11). The relatively high phonon energy of glass matrix enables rather efficient nonradiative decay from $^4S_{3/2}$ to lower emitting states and results in a fast luminescence decay, however, in the low phonon environment of $Ba_4RE_3F_{17}$ radiative transitions are predominant. The luminescence spectrum corresponding to the fast decay consists of broad bands characteristic to Er^{3+} ions in the amorphous environment. Sharp and narrow peaks corresponding to the slow decay indicate the luminescence of Er^{3+} ions in the crystalline environment. The results suggest that Er^{3+} ions are incorporated both in the fluoride nanocrystals and glass matrix. This effect can be used to compare the Er^{3+} distribution in different glass ceramics. In the glass ceramics with similar $Ba_4RE_3F_{17}$ nanocrystals variations in the relative intensity of the slow and fast decay were detected.

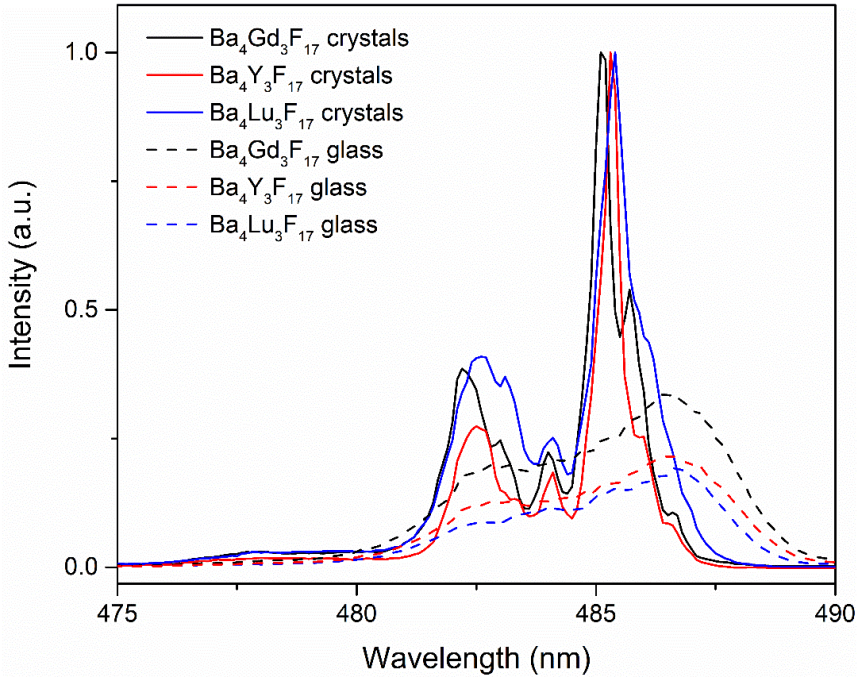

Fig. 12 Time-resolved excitation spectra (exciting $^4F_{7/2}$, detecting integral green emission of Er^{3+} in nanocrystals and glass phase) of glass ceramics containing $Ba_4Gd_3F_{17}$, $Ba_4Y_3F_{17}$ and $Ba_4Lu_3F_{17}$ nanocrystals, doped with 1% ErF_3 measured at 10 K.

The time-resolved excitation spectra of Er^{3+} ions in the glassy and crystalline environment of the glass ceramics containing $Ba_4Gd_3F_{17}$, $Ba_4Y_3F_{17}$ and $Ba_4Lu_3F_{17}$ nanocrystals are shown in Fig. 12. The relative luminescence intensity of Er^{3+} in the glass and crystalline phase were calculated for each glass ceramics. In glass ceramics containing $Ba_4Lu_3F_{17}$ the relative intensity of Er^{3+} ions in the glass phase was found to be approximately 14% lower than in $Ba_4Y_3F_{17}$ and 36 % lower than in $Ba_4Gd_3F_{17}$ containing glass ceramics. The results suggest that the Lu^{3+} containing matrix exhibits superior incorporation efficiency of Er^{3+} ions in comparison to similar $Ba_4RE_3F_{17}$ hosts. The results confirm the hypothesis that the incorporation efficiency of the activator ions strongly depends on the chemical composition of the crystalline phase and follows the trend Gd>Y,Er>Lu.

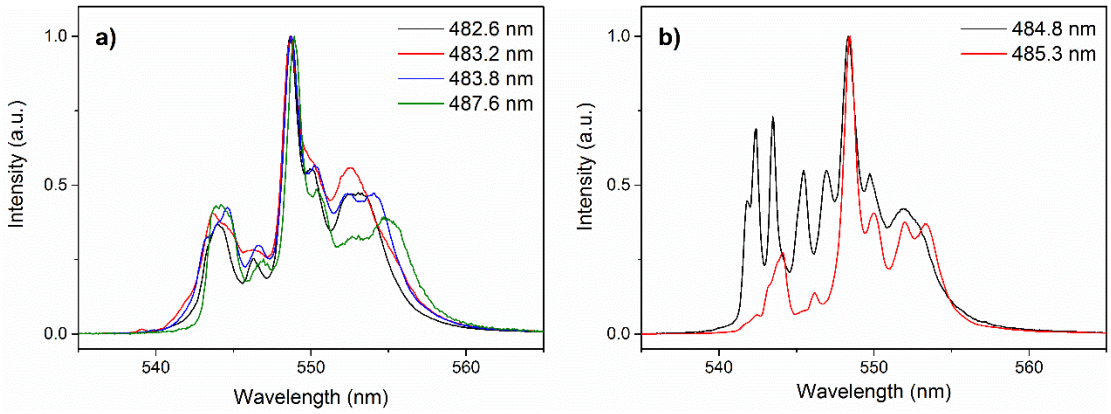

Fig. 13. Luminescence spectra of Er^{3+} ions in glass ceramics heat treated at a) 550°C and b) 700°C for 2 h detected at 10 K.

The time-resolved site-selective spectroscopy can be used not only for selective excitation of Er^{3+} ions in the glass and nanocrystals, but also for the detection of the changes in the local structure of Er^{3+} ions in the crystalline lattice. Considerable differences were detected for the glass ceramics heat treated at low and high temperature. In the glass ceramics heat treated at 550°C for 2 h multiple similar but not identic luminescence spectra corresponding to the Er^{3+} ions in the fluoride nanocrystals could be observed indicating the incorporation of the activator ions in distorted environment (see Fig. 13 a). However, in the glass ceramics heat treated at 700°C for 2 h two distinct spectra associated with the Er^{3+} ions in nanocrystals can be detected (see Fig. 13 b). As mentioned previously, two polymorphic modifications are known for $Ba_4Lu_3F_{17}$ – with cubic fluorite and rhombohedrally distorted fluorite structure. Both phases are structurally similar, but the structural elements in the cubic phase are expected to be distorted unlike the ordered rhombohedral $Ba_4Lu_3F_{17}$ phase [16]. The distortion of the structural elements should result in the deviations of the local environment of Er^{3+} ions in the fluorite type phase and lead to formation of many similar Er^{3+} positions in the fluorite lattice. This effect is detected in the glass ceramics heat treated at 550°C for 2 h suggesting the formation of the cubic phase in these materials.

The changes in the local environment of Er^{3+} ions in the $Ba_4Lu_3F_{17}$ heat treat at 700°C for 2 h can be explained with the phase transition to the rhombohedral modification. To our best knowledge, there are no reports of the atomic positions and unit cell parameters of rhombohedral $Ba_4Lu_3F_{17}$, therefore we performed the analysis of the polycrystalline samples using Rietveld refinement. The atomic positions of $Ba_4Y_3F_{17}$ reported in [36] were used and were found to be in a good agreement with the rhombohedral $Ba_4Lu_3F_{17}$. Rhombohedral cell (space-group: $R\bar{3}$) with a = b = 10.981 Å and c = 20.229 Å was obtained and the unit cell parameters are in a good agreement with the theoretical model (goodness of fit $\chi^2 = 2.35$). The XRD pattern and atomic positions of rhombohedral $Ba_4Lu_3F_{17}$ are shown in the appendix. In the structural model of rhombohedral $Ba_4Lu_3F_{17}$ there are three distinct cationic positions – two Ba^{2+} and one Lu^{3+} position. Due to similarity of ionic radii of Lu^{3+} and Er^{3+}, the erbium ions are expected to replace Lu^{3+} positions. The incorporation of Er^{3+} ions in a single crystallographic position in $Ba_4Gd_3F_{17}$ and $Ba_4Y_3F_{17}$ was reported previously

[25,26]. However, in the glass ceramics containing $Ba_4Lu_3F_{17}$ two distinct Er^{3+} positions were detected using site selective spectroscopy (see Fig. 13 b). The structural model of rhombohedral $Ba_4Lu_3F_{17}$ consists of $Ba_8Lu_6F_{68}$ structural units (rare earth octahedral superclusters) arranged in layers. It is the most common structural unit found in BaF_2-REF_3 fluorite and fluorite related phases [16]. Nevertheless, in fluorite type BaF_2-REF_3 (RE=Yb-Lu) phases new type of structural unit $RE_8Ba_6F_{71}$ (octahedral alkali earth supercluster) was recently discovered [37]. Indeed, two distinct Er^{3+} sites were also found in the rhombohedral $Ba_4Yb_3F_{17}$ [27]. Despite the good agreement of the proposed structural model of $Ba_4Lu_3F_{17}$ with the experimental data, the coexistence of two distinct Er^{3+} position in $Ba_4Lu_3F_{17}$ agrees well with the formation of different, structurally similar superclusters in the structure. For the confirmation of the coexistence of different superclusters in $Ba_4Lu_3F_{17}$, further investigation is required.

The results of site-selective spectroscopy of Er^{3+} ions indicate the formations of two modifications of $Ba_4Lu_3F_{17}$ – cubic at low temperatures and rhombohedral at high temperatures. Such changes agree well with DTA, XRD, SEM and UCL data. To detect the phase transition from cubic to rhombohedral phase, precursor glass and glass ceramics heat treated at 550-700°C for 2 h were analysed and compared with polycrystalline Er^{3+} doped $Ba_4Lu_3F_{17}$.

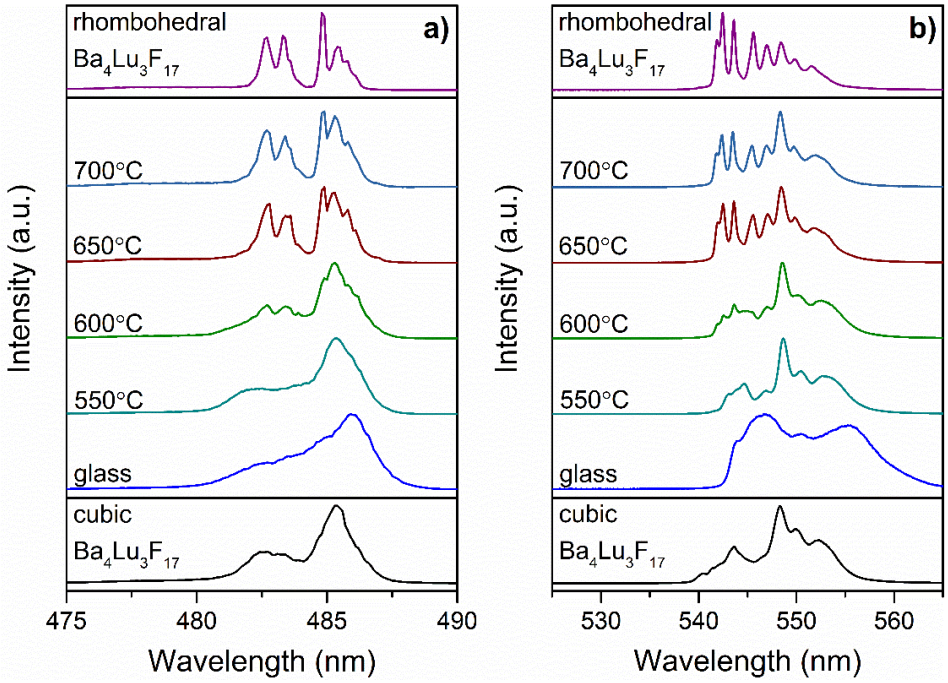

Fig. 14. a) Excitation spectra (exciting $^4F_{7/2}$, detecting 545.2 nm emission) and b) emission spectra (excited with 484.8 nm) of Er^{3+} ions in glass ceramics doped with 0.1% ErF_3 compared with polycrystalline cubic and rhombohedral $Ba_4Lu_3F_{17}$ measured at 10 K.

Fig. 14 shows the excitation and emission spectra of glass ceramics doped with 0.1% ErF_3 compared to polycrystalline cubic and rhombohedral Er^{3+} doped $Ba_4Lu_3F_{17}$. For the precursor glass broad excitation and emission bands confirm the incorporation of Er^{3+} ions in the amorphous environment. The thermal treatment promotes the

formation of the crystalline phases as the result narrow luminescence bands characteristic to the crystalline environment are detected. After heat treatment at 500-600°C both excitation and emission spectra closely resemble the spectra characteristic to Er^{3+} ions in cubic $Ba_4Lu_3F_{17}$. The heat treatment at 650-700°C results in considerable changes in the spectra indicating the formation of the rhombohedral $Ba_4Lu_3F_{17}$. The results suggest that in the investigated glass ceramics metastable cubic phase is formed at low temperatures and after the heat treatment at approximately 600-650°C a phase transition from cubic to rhombohedral phase takes place. The site-selective spectroscopy data are in a good agreement with the DTA (see Fig. 1) that indicate an exothermic effect located at 638±6 °C associated with the phase transition.

Conclusions

In this research novel transparent Er^{3+} doped oxyfluoride glass ceramics containing $Ba_4Lu_3F_{17}$ nanocrystals have been prepared. The analysis of the local environment of Er^{3+} in the fluoride nanocrystals using site-selective spectroscopy revealed the phase transition from metastable cubic to rhombohedral $Ba_4Lu_3F_{17}$ after the heat treatment at 600-650°C.

Exceptionally efficient incorporation of Er^{3+} ions in the rhombohedral phase was detected. The Er^{3+} content in $Ba_4Lu_3F_{17}$ was estimated to be higher by 14% and 36% in comparison to erbium doped glass ceramics containing $Ba_4Y_3F_{17}$ and $Ba_4Gd_3F_{17}$ nanocrystals, respectively. The results suggest preferential incorporation of rare earth ions with larger ionic radii (Er^{3+}) in the hosts containing smaller rare earth ions (such as Lu^{3+}).

In conclusion, rhombohedral $Ba_4Lu_3F_{17}$ in the glass ceramics was proven to be a suitable host for Er^{3+} ions combining low phonon energy and excellent incorporation efficiency of Er^{3+} ions in the crystalline phase resulting in the intense upconversion luminescence.

Acknowledgements

The authors wish to express gratitude to R. Ignatans for Rietveld refinement. This work was supported by National Research Program IMIS^2 and Arnis Riekstins "MikroTik" donation. Donations are administered by the University of Latvia Foundation.

References

[1] B.N. Samson, P. a Tick, N.F. Borrelli, Efficient neodymium-doped glass-ceramic fiber laser and amplifier, Opt. Lett. 26 (2001) 145. doi:10.1364/OL.26.000145.

[2] D. Chen, Z. Wan, S. Liu, Highly Sensitive Dual-Phase Nanoglass-Ceramics Self-Calibrated Optical Thermometer, Anal. Chem. 88 (2016) 4099–4106. doi:10.1021/acs.analchem.6b00434.

[3] S. Jiang, P. Zeng, L. Liao, S. Tian, H. Guo, Y. Chen, C. Duan, M. Yin, Optical thermometry based on upconverted luminescence in transparent glass ceramics containing $NaYF_4$:Yb^{3+} /Er^{3+} nanocrystals, J. Alloys Compd. 617 (2014) 538–541. doi:10.1016/j.jallcom.2014.08.080.

[4] G. Lee, N. Savage, B. Wagner, Y. Zhang, B. Jacobs, H. Menkara, C. Summers, Z. Kang, Synthesis and luminescence properties of transparent nanocrystalline GdF_3:Tb glass-ceramic scintillator, J. Lumin. 147 (2014) 363–366. doi:10.1016/j.jlumin.2013.11.073.

[5] M.B. Beckert, S. Gallego, Y. Ding, E. Elder, J.H. Nadler, Medical imaging scintillators from glass-ceramics using mixed rare-earth halides, Opt. Mater. (Amst). 60 (2016) 513–520. doi:10.1016/j.optmat.2016.09.015.

[6] Z. Chen, L. Sun, H. Zhang, G.P. Dong, M. Gecevicius, Y.Q. Liu, Y.X. Fu, C. Jiang, S.F. Zhou, J.R. Qiu, Near-infrared wavelength-dependent nonlinear transmittance tailoring in glass ceramics containing Er^{3+}:LaF_3 nanocrystals, J. Mater. Chem. C. 4 (2016) 6707–6712. doi:10.1039/C6TC01876A.

[7] E. Pavel, M. Mihailescu, V.B. Nicolae, S. Jinga, E. Andronescu, E. Rotiu, L. Ionescu, C. Mazilu, Holographic testing of fluorescent photosensitive glass–ceramics, Opt. Commun. 284 (2011) 930–933. doi:10.1016/j.optcom.2010.10.023.

[8] K.V. Krishnaiah, E. Soares de Lima Filho, Y. Ledemi, G. Nemova, Y. Messaddeq, R. Kashyap, Development of ytterbium-doped oxyfluoride glasses for laser cooling applications, Sci. Rep. 6 (2016) 21905. doi:10.1038/srep21905.

[9] Y. Ledemi, A.-A. Trudel, V. a G. Rivera, S. Chenu, E. Véron, L.A. Nunes, M. Allix, Y. Messaddeq, White light and multicolor emission tuning in triply doped Yb^{3+}/Tm^{3+}/Er^{3+} novel fluoro-phosphate transparent glass-ceramics, J. Mater. Chem. C. 2 (2014) 5046–5056. doi:10.1039/C4TC00455H.

[10] D. Chen, Y. Wang, K. Zheng, T. Guo, Y. Yu, P. Huang, Bright upconversion white light emission in transparent glass ceramic embedding Tm^{3+}/Er^{3+}/Yb^{3+}:β-YF_3 nanocrystals, Appl. Phys. Lett. 91 (2007) 251903. doi:10.1063/1.2825285.

[11] P.P. Fedorov, A.A. Luginina, A.I. Popov, Transparent oxyfluoride glass ceramics, J. Fluor. Chem. 172 (2015) 22–50. doi:10.1016/j.jfluchem.2015.01.009.

[12] A. de Pablos-Martín, A. Durán, M.J. Pascual, Nanocrystallisation in oxyfluoride systems: mechanisms of crystallisation and photonic properties, Int. Mater. Rev. 57 (2012) 165–186. doi:10.1179/1743280411Y.0000000004.

[13] F. Auzel, Upconversion and Anti-Stokes Processes with f and d Ions in Solids, Chem. Rev. 104 (2004) 139–174. doi:10.1021/cr020357g.

[14] J.C. Goldschmidt, S. Fischer, Upconversion for Photovoltaics - a Review of Materials, Devices and Concepts for Performance Enhancement, Adv. Opt. Mater. 3 (2015) 510–535. doi:10.1002/adom.201500024.

[15] M.P. Miller, J.C. Wright, Single site multiphonon and energy transfer relaxation phenomena in $BaF_2:Er^{3+}$, J. Chem. Phys. 68 (1978) 1548–1562. doi:10.1063/1.435924.

[16] P.P. Fedorov, Association of point defects in non-stoichiometric $M_{1-x}R_xF_{2+x}$ fluorite-type solid solutions, Butll. Soc. Cat. Cien. XII (1991) 349–381.

[17] B.P. Sobolev, Nonstoichiometry in inorganic fluorides: I. Nonstoichiometry in MF_m-RF_n ($m < n \leq 4$) systems, Crystallogr. Reports. 57 (2012) 434–454. doi:10.1134/S1063774512030194.

[18] N.L. Tkachenko, L.S. Garashina, O.E. Izotova, V.B. Aleksandrov, B.P. Sobolev, Phase equilibria in BaF_2-(Y, Ln)F_3 systems, J. Solid State Chem. 8 (1973) 213–218. doi:10.1016/0022-4596(73)90087-X.

[19] M. Kieser, O. Greis, Preparation, thermal characterization and x-ray powder diffraction of Ba_2REF_7 superstructure phases (RE≡Dy-Lu, Y), J. Less Common Met. 71 (1980) 63–69. doi:10.1016/0022-5088(80)90101-0.

[20] H.K. Dan, D. Zhoua, W. Rongfei, T.M. Hau, Q. Jiao, X. Yu, J. Qiu, Up-conversion of Er^{3+}/Yb^{3+} co-doped transparent glass-ceramics containing Ba_2LaF_7 nanocrystals, J. Rare Earths. 31 (2013) 843–848. doi:10.1016/S1002-0721(12)60368-8.

[21] K. Biswas, S. Balaji, D. Ghosh, A. Kalyandurg, Enhanced near-infrared to green upconversion from Er^{3+}-doped oxyfluoride glass and glass ceramics containing $BaGdF_5$ nanocrystals, Int. J. Appl. Glas. Sci. 8 (2017) 204–215. doi:10.1111/ijag.12241.

[22] M. Gu, Q.-C. Gao, S.-M. Huang, X.-L. Liu, B. Liu, C. Ni, Luminescence properties of Pr^{3+}-doped transparent oxyfluoride glass–ceramics containing $BaYF_5$ nanocrystals, J. Lumin. 132 (2012) 2531–2536. doi:10.1016/j.jlumin.2012.04.043.

[23] S. Jiang, H. Guo, X. Wei, C. Duan, M. Yin, Enhanced upconversion in Ho^{3+}-doped transparent glass ceramics containing $BaYbF_5$ nanocrystals, J. Lumin. 152 (2014) 195–198. doi:10.1016/j.jlumin.2013.11.030.

[24] J. Yang, H. Guo, X. Liu, H.M. Noh, J.H. Jeong, Down-shift and up-conversion luminescence in $BaLuF_5:Er^{3+}$ glass–ceramics, J. Lumin. 151 (2014) 71–75. doi:10.1016/j.jlumin.2014.02.007.

[25] G. Krieke, A. Sarakovskis, R. Ignatans, J. Gabrusenoks, Phase transitions and upconversion luminescence in oxyfluoride glass ceramics containing $Ba_4Gd_3F_{17}$ nanocrystals, J. Eur. Ceram. Soc. 37 (2017) 1713–1722. doi:10.1016/j.jeurceramsoc.2016.12.023.

[26] G. Krieke, A. Sarakovskis, Crystallization and upconversion luminescence of distorted fluorite nanocrystals in Ba^{2+} containing oxyfluoride glass ceramics, J.

Eur. Ceram. Soc. 36 (2016) 1715–1722. doi:10.1016/j.jeurceramsoc.2016.01.025.

[27] G. Krieke, A. Sarakovskis, M. Springis, Ordering of fluorite-type phases in erbium-doped oxyfluoride glass ceramics, J. Eur. Ceram. Soc. 38 (2018) 235–243. doi:10.1016/j.jeurceramsoc.2017.08.037.

[28] T.. Kiczenski, L.-S. Du, J.F. Stebbins, F-19 NMR study of the ordering of high field strength cations at fluoride sites in silicate and aluminosilicate glasses, J. Non. Cryst. Solids. 337 (2004) 142–149. doi:10.1016/j.jnoncrysol.2004.03.123.

[29] I. V. Veksler, A.M. Dorfman, M. Kamenetsky, P. Dulski, D.B. Dingwell, Partitioning of lanthanides and Y between immiscible silicate and fluoride melts, fluorite and cryolite and the origin of the lanthanide tetrad effect in igneous rocks, Geochim. Cosmochim. Acta. 69 (2005) 2847–2860. doi:10.1016/j.gca.2004.08.007.

[30] G. Krieke, A. Sarakovskis, M. Springis, Upconversion luminescence of a transparent glass ceramics with hexagonal Na(Gd ,Lu)F_4 nanocrystals, J. Alloys Compd. 694 (2017) 952–958. doi:10.1016/j.jallcom.2016.10.156.

[31] N. Jiang, S. Zhou, D. Su, J. Qiu, Do Eu dopants prefer the precipitated LaF_3 nanocrystals in glass ceramics?, Phys. Status Solidi - Rapid Res. Lett. 6 (2012) 487–489. doi:10.1002/pssr.201206476.

[32] A. de Pablos-Martín, M.A. García, A. Muñoz-Noval, G.R. Castro, M.J. Pascual, A. Durán, Analysis of the distribution of Tm^{3+} ions in LaF_3 containing transparent glass-ceramics through X-ray absorption spectroscopy, J. Non. Cryst. Solids. 384 (2014) 83–87. doi:10.1016/j.jnoncrysol.2013.07.021.

[33] B.P. Sobolev, Nonstoichiometry in inorganic fluorides: I. Nonstoichiometry in MF_m-RF_n ($m < n \leq 4$) systems, Crystallogr. Reports. 57 (2012) 434–454. doi:10.1134/S1063774512030194.

[34] S. V Kuznetsov, P.P. Fedorov, V. V Voronov, K.S. Samarina, R.P. Ermakov, V. V Osiko, Synthesis of $Ba_4R_3F_{17}$ (R stands for rare-earth elements) powders and transparent compacts on their base, Russ. J. Inorg. Chem. 55 (2010) 484–493. doi:10.1134/S0036023610040029.

[35] M. Pollnau, D.R. Gamelin, S.R. Lüthi, H.U. Güdel, M.P. Hehlen, Power dependence of upconversion luminescence in lanthanide and transition-metal-ion systems, Phys. Rev. B. 61 (2000) 3337–3346. doi:10.1103/PhysRevB.61.3337.

[36] B.A. Maksimov, K. Solans, A.P. Dudka, E.A. Genkina, M. Font-Badria, I.I. Buchinskaya, A.A. Loshmanov, A.M. Golubev, V.I. Simonov, M. Font-Altaba, others, The fluorite-matrix-based $Ba_4R_3F_{17}$ (R= Y, Yb) crystal structure. Ordering of cations and specific features of the anionic motif, Crystallogr. Rep. 41 (1996) 50–57.

[37] B.P. Sobolev, A.M. Golubev, L.P. Otroshchenko, V.N. Molchanov, R.M. Zakalyukin, E.A. Ryzhova, P. Herrero, $Ba_{1-x}R_xF_{2+x}$ Phases (R = Gd-Lu) with distorted fluorite-type structures—products of crystallization of incongruent melts in the BaF_2-RF_3 Systems (R = Gd-Lu). III. Defect $Ba_{0.75}Lu_{0.25}F_{2.25}$ structure. A new $\{Lu_8[Ba_6F_{71}]\}$ supercluster of defects, Crystallogr. Reports.

48 (2003) 944–952. doi:10.1134/1.1627436.

Appendix

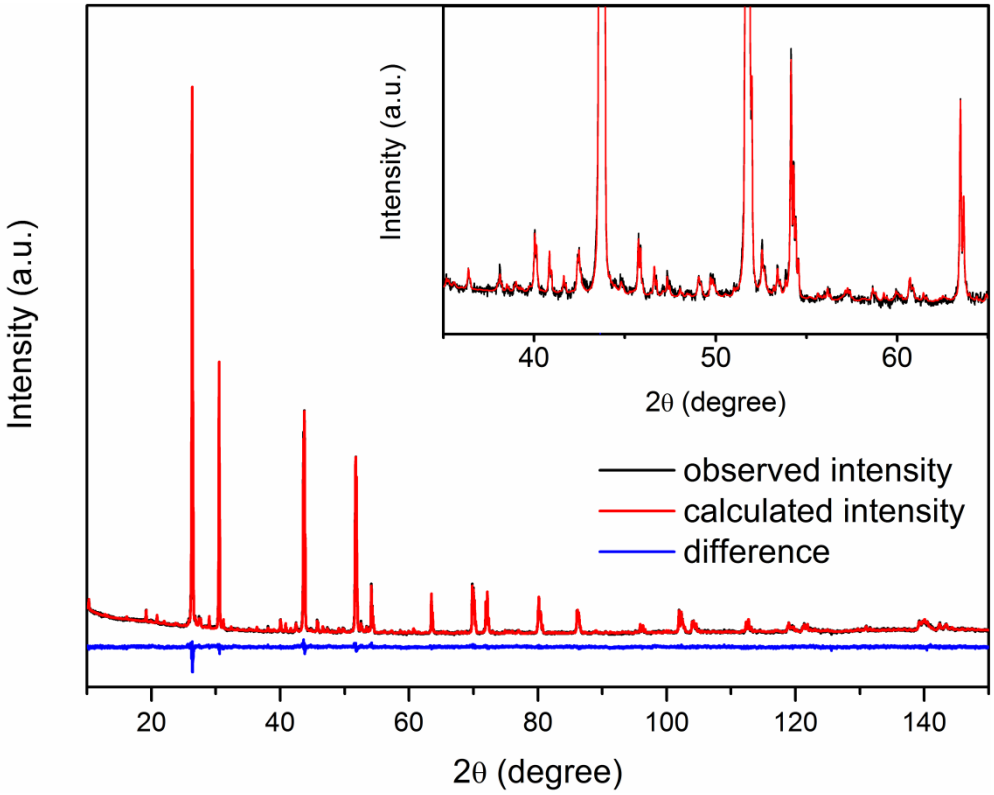

Experimental and calculated XRD pattern of $Ba_4Lu_3F_{17}$. Inset: enlarged section of XRD pattern.

Atomic parameters of the structure model (space-group: R (No. 148))

Atom	Ox	Wyckoff position	Site symmetry	x	y	z	Occ.
F	-1	f18	1	0.9640	0.9297	0.4877	0.1666
Ba	2	f18	1	0.2293	0.0295	0.0843	1
F	-1	f18	1	0.0428	0.7876	0.0443	1
F	-1	f18	1	0.4604	0.0737	0.0386	1
F	-1	f18	1	0.4261	0.2963	0.1203	1
Lu	3	f18	1	0.0880	0.6144	0.0828	1
F	-1	f18	1	0.2040	0.5044	0.0529	1
F	-1	a3	-3	0	0	0	1
Ba	2	c6	3	0	0	0.2684	1
F	-1	f18	1	0.2385	0.3671	0.1749	1
F	-1	c6	3	0	0	0.1431	1

Figure captions

Fig. 1. DTA curves of precursor glasses doped with 0.1-3% ErF_3.

Fig. 2. XRD patterns of the precursor glass and glass ceramics with a) 0.1% ErF_3 and b) 1.0% ErF_3 heat treated at different temperatures for 2 h.

Fig. 3. XRD patterns of the glass ceramics with 0.1% ErF_3 heat treated at 700°C for 2 h and polycrystalline rhombohedral $Ba_4Lu_3F_{17}$ (superstructure peaks are marked with *).

Fig. 4. SEM micrographs of glass and glass ceramics heat treated at 600-700°C 2 h doped with 0.1 % ErF_3 (a-d) and 1% ErF_3 (e-h).

Fig. 5. UCL spectra under 975 nm excitation of the precursor glass and glass ceramics doped with 0.1% ErF_3 heat treated at 550-700^{0}C for 2 h.

Fig. 6. a) UCL spectra of glass ceramics doped with 0.1-3% ErF_3 heat treated at 650°C for 2 h under 975 nm excitation and b) Luminescence decay of green emission under 975 nm excitation. Inset: effective lifetime of the green emission excited at 975 nm and 520 nm.

Fig. 7. Photographs of glass ceramics doped with 0.1-3 mol% ErF_3 heat treated at 650^{0}C for 2 h: a) as prepared, b) excited with 975 nm continuous wave laser.

Fig. 8. Power dependence of the green ($^4S_{3/2}\rightarrow {}^4I_{15/2}$) and red ($^4F_{9/2}\rightarrow {}^4I_{15/2}$) UCL emission in the glass ceramics doped with a) 0.1% and b) 3% ErF_3 under 975 nm excitation.

Fig. 9. Partial energy level diagram of Er^{3+} ions and dominant UCL mechanisms in the glass ceramics.

Fig. 10. The effective decay time of $^4S_{3/2}\rightarrow {}^4I_{15/2}$ emission and red/green emission ratio of Er^{3+} in polycrystalline $Ba_4Lu_3F_{17}$, excited at 445 nm. x and droplines mark the values of glass ceramics heat treated at 700°C for 2 h.

Fig. 11. Time-resolved luminescence spectra of the glass ceramics heat treated at 700°C for 2 h doped with 1% ErF_3 containing $Ba_4Lu_3F_{17}$ nanocrystals corresponding to the fast (50 ns – 150 ns) and slow (10.0 μs – 10.1 μs) components. Luminescence was excited at 489 nm, measured at 10 K. Inset: luminescence decay of Er^{3+} ions in glass ceramics heat treated at 700°C for 2 h doped with 1% ErF_3 excited at 489 nm, measured at 10 K.

Fig. 12. Time-resolved excitation spectra (exciting $^4F_{7/2}$, detecting integral green emission of Er^{3+} in nanocrystals and glass phase) of glass ceramics containing $Ba_4Gd_3F_{17}$, $Ba_4Y_3F_{17}$ and $Ba_4Lu_3F_{17}$ nanocrystals, doped with 1% ErF_3 measured at 10 K.

Fig. 13. Luminescence spectra of Er^{3+} ions in glass ceramics heat treated at a) 550°C and b) 700°C for 2 h detected at 10 K.

Fig. 14. a) Excitation spectra (exciting $^4F_{7/2}$, detecting 545.2 nm emission) and b) emission spectra (excited with 484.8 nm) of Er^{3+} ions in glass ceramics doped with

0.1% ErF_3 compared with polycrystalline cubic and rhombohedral $Ba_4Lu_3F_{17}$ measured at 10 K.

Institute of Solid State Physics, University of Latvia as the Center of Excellence has received funding from the European Union's Horizon 2020 Framework Programme H2020-WIDESPREAD-01-2016-2017-TeamingPhase2 under grant agreement No. 739508, project CAMART²

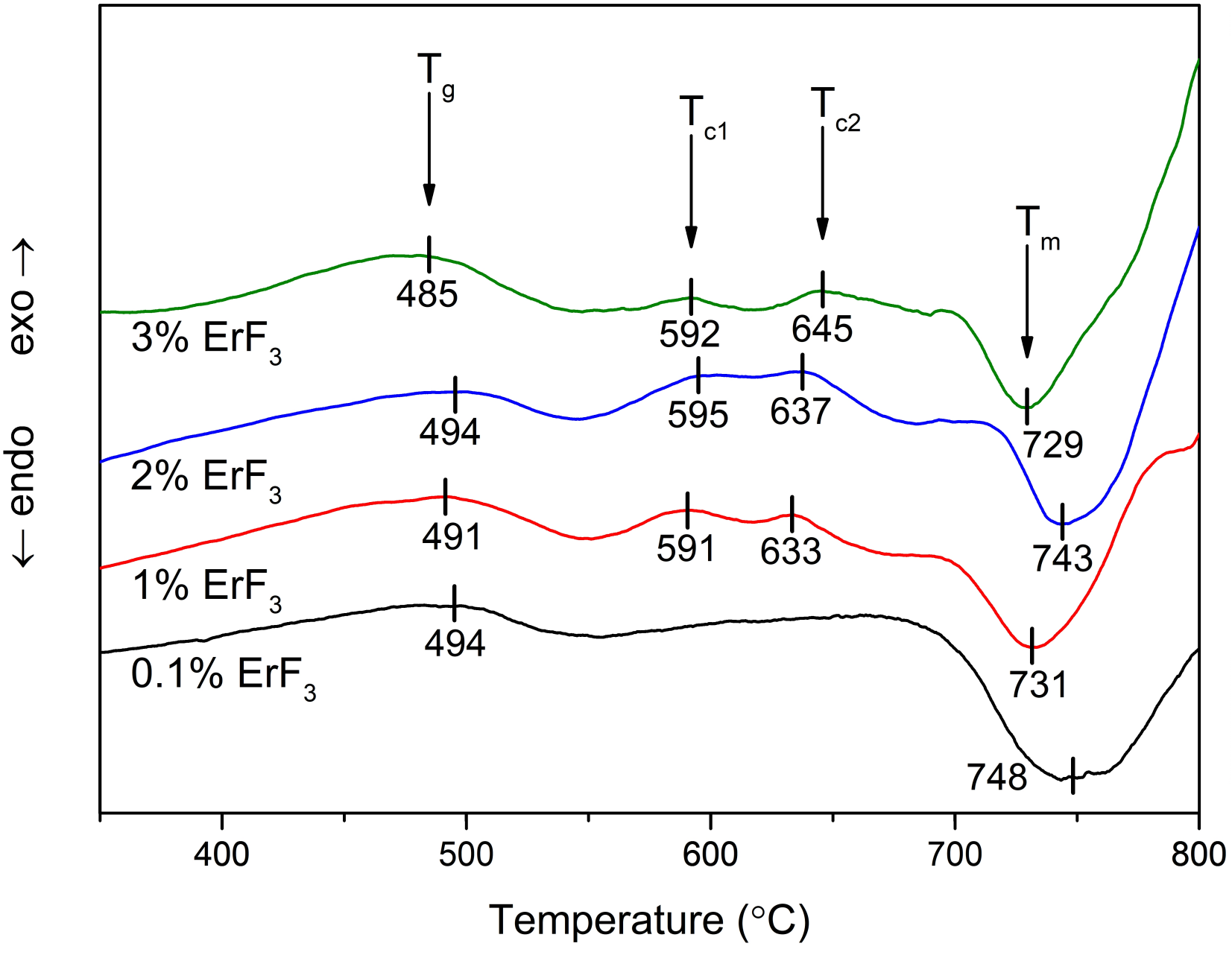
T g
T c1
T c2
T m
485
592
645
729
3% ErF 3
494
595
637
2% ErF 3
491
591
633
743
1% ErF 3
494
731
0.1% ErF 3
748
← endo exo →
400
500
600
700
800
Temperature (°C)

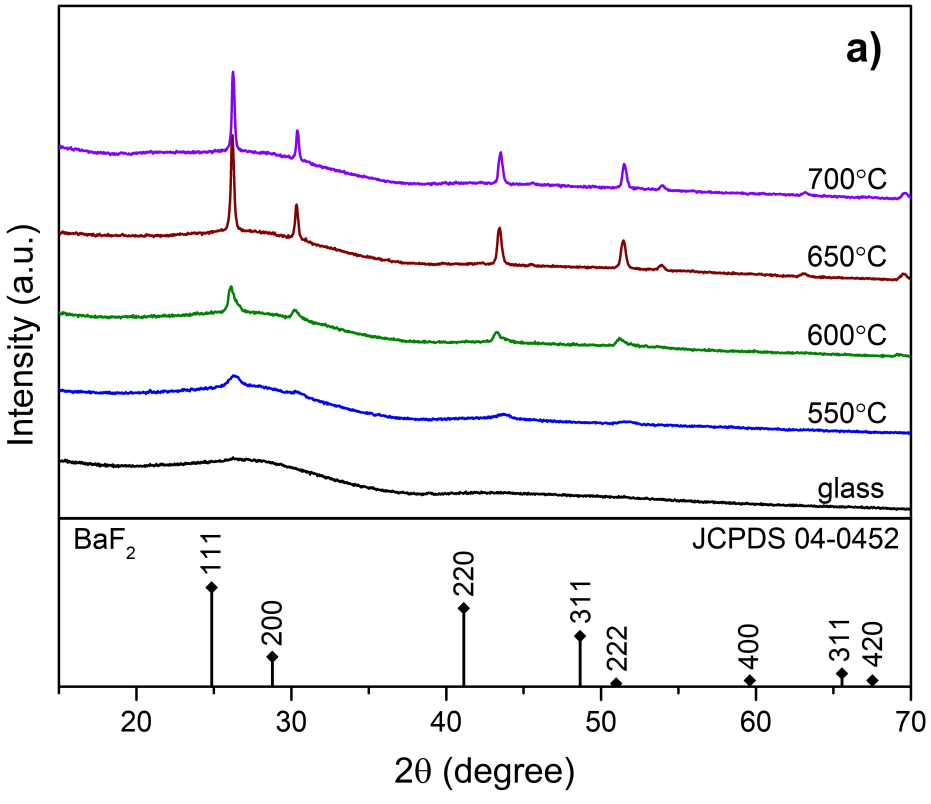
a)
Intensity (a.u.)
700°C
650°C
600°C
550°C
glass
BaF2
JCPDS 04-0452
111
200
220
311
222
400
311
420
20
30
40
50
60
70
2θ (degree)

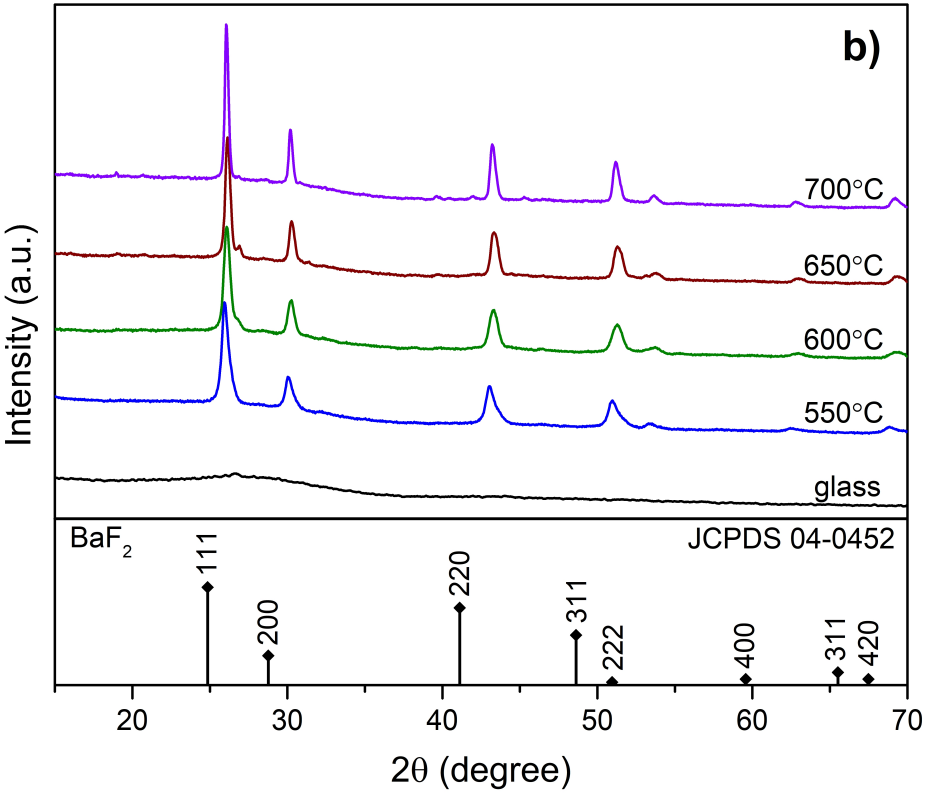
b)
Intensity (a.u.)
700°C
650°C
600°C
550°C
glass
BaF2
JCPDS 04-0452
111
200
220
311
222
400
311
420
20
30
40
50
60
70
2θ (degree)

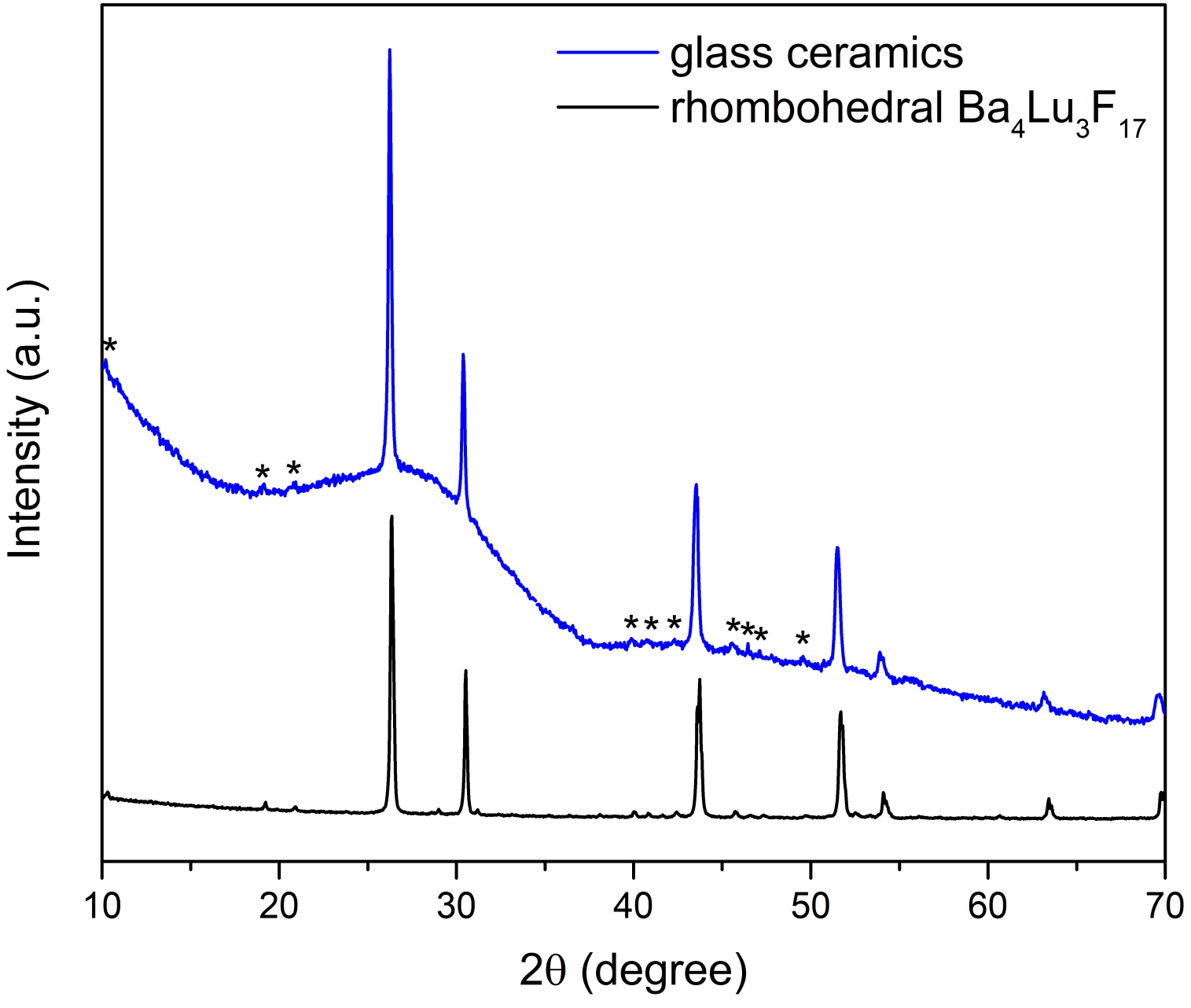
glass ceramics
rhombohedral $Ba_4Lu_3F_{17}$
Intensity (a.u.)
2θ (degree)
10
20
30
40
50
60
70
*
* *
* * *
* * *
*

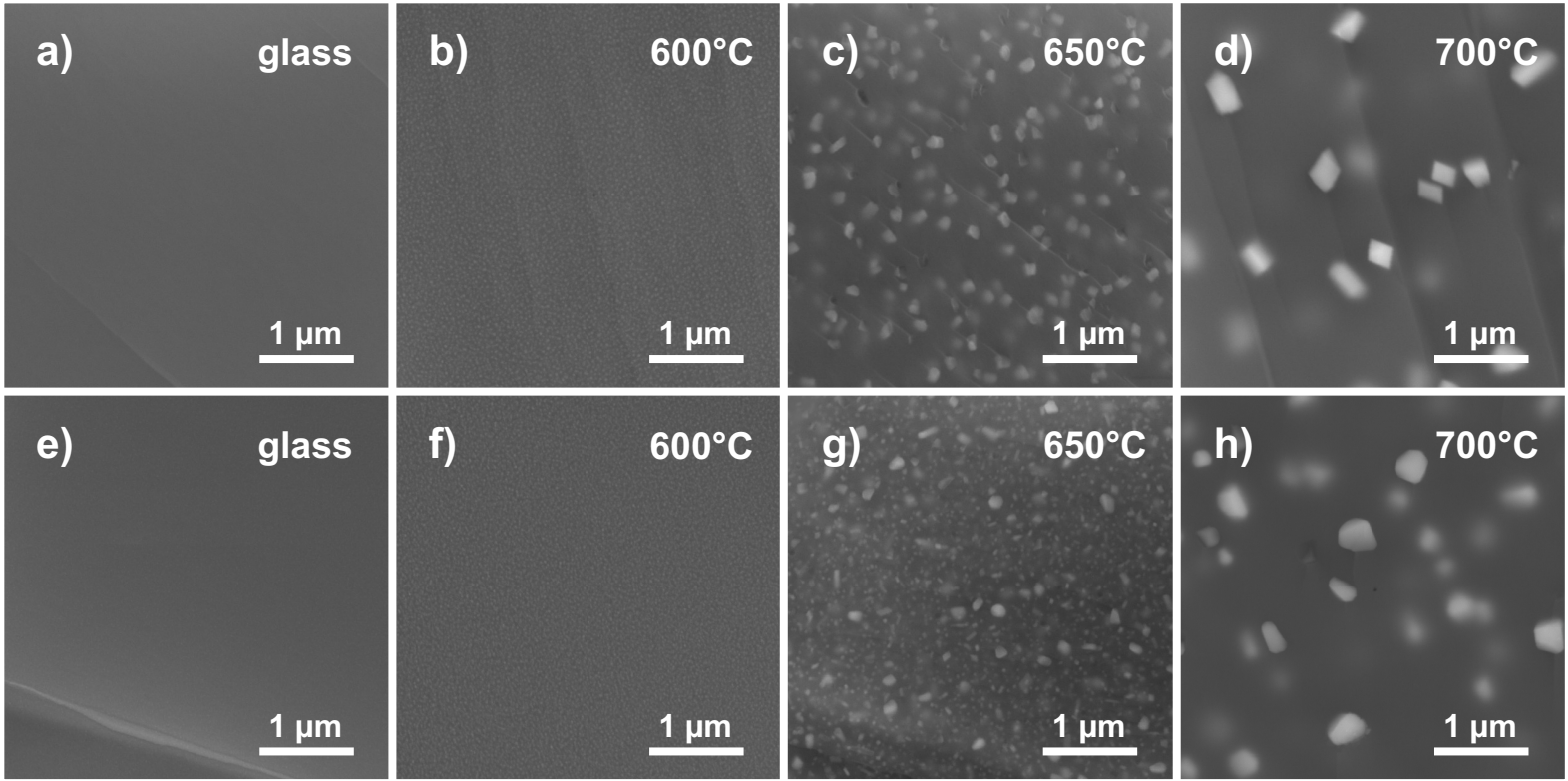
a)
glass
1 µm
b)
600°C
1 µm
c)
650°C
1 µm
d)
700°C
1 µm
e)
glass
1 µm
f)
600°C
1 µm
g)
650°C
1 µm
h)
700°C
1 µm

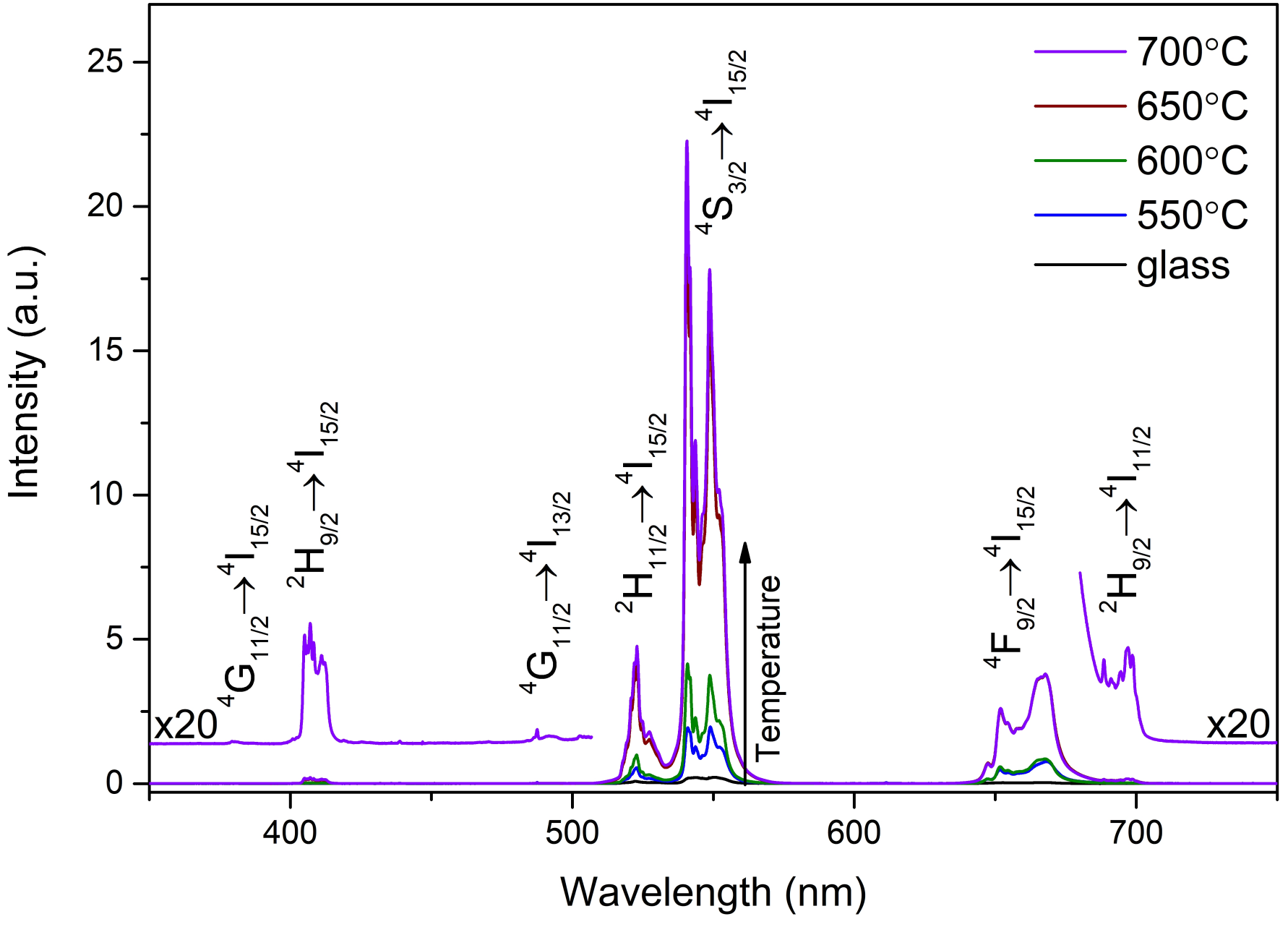
Intensity (a.u.)
Wavelength (nm)
0
5
10
15
20
25
400
500
600
700
700°C
650°C
600°C
550°C
glass
x20
x20
$^4G_{11/2}\rightarrow{}^4I_{15/2}$
$^2H_{9/2}\rightarrow{}^4I_{15/2}$
$^4G_{11/2}\rightarrow{}^4I_{13/2}$
$^2H_{11/2}\rightarrow{}^4I_{15/2}$
$^4S_{3/2}\rightarrow{}^4I_{15/2}$
$^4F_{9/2}\rightarrow{}^4I_{15/2}$
$^2H_{9/2}\rightarrow{}^4I_{11/2}$
Temperature

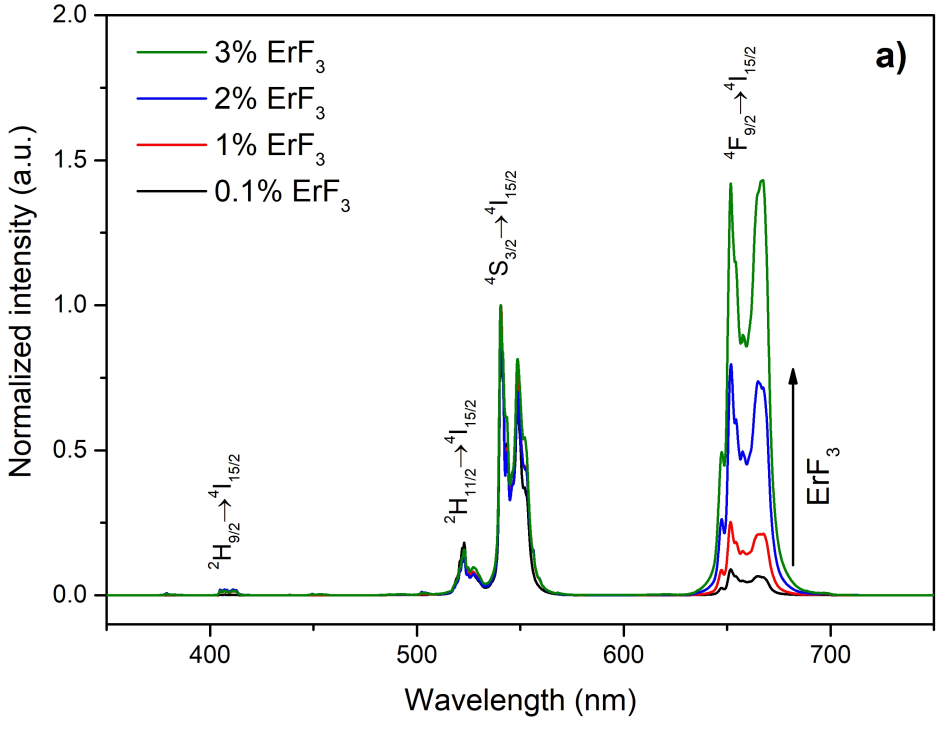
a)
3% ErF3
2% ErF3
1% ErF3
0.1% ErF3
Normalized intensity (a.u.)
Wavelength (nm)
2H9/2→4I15/2
2H11/2→4I15/2
4S3/2→4I15/2
4F9/2→4I15/2
ErF3

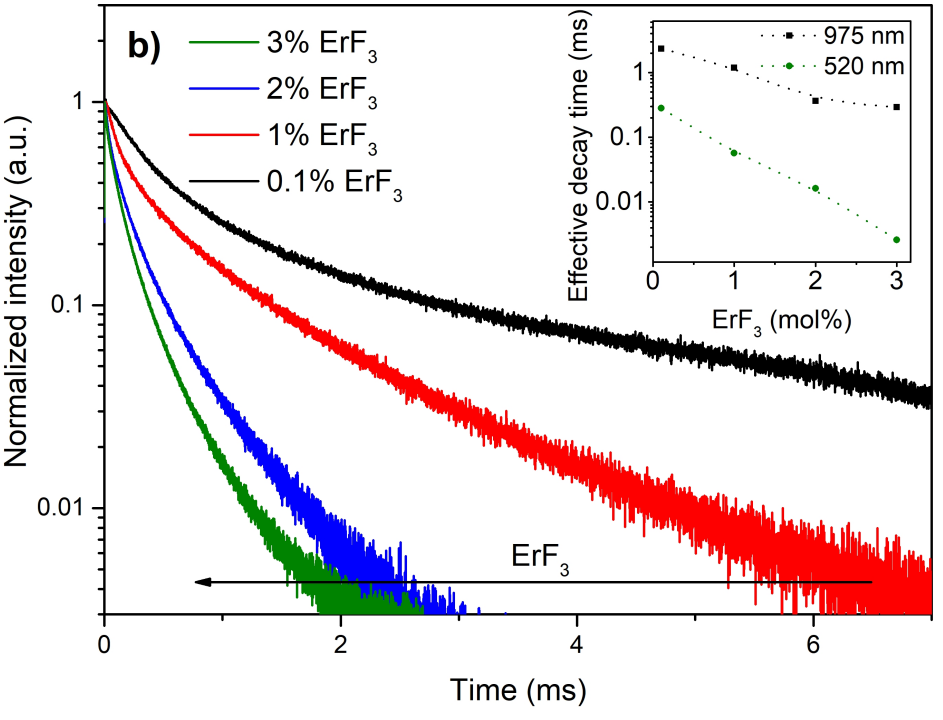
b)
3% ErF3
2% ErF3
1% ErF3
0.1% ErF3
Normalized intensity (a.u.)
Time (ms)
ErF3
Effective decay time (ms)
975 nm
520 nm
ErF3 (mol%)

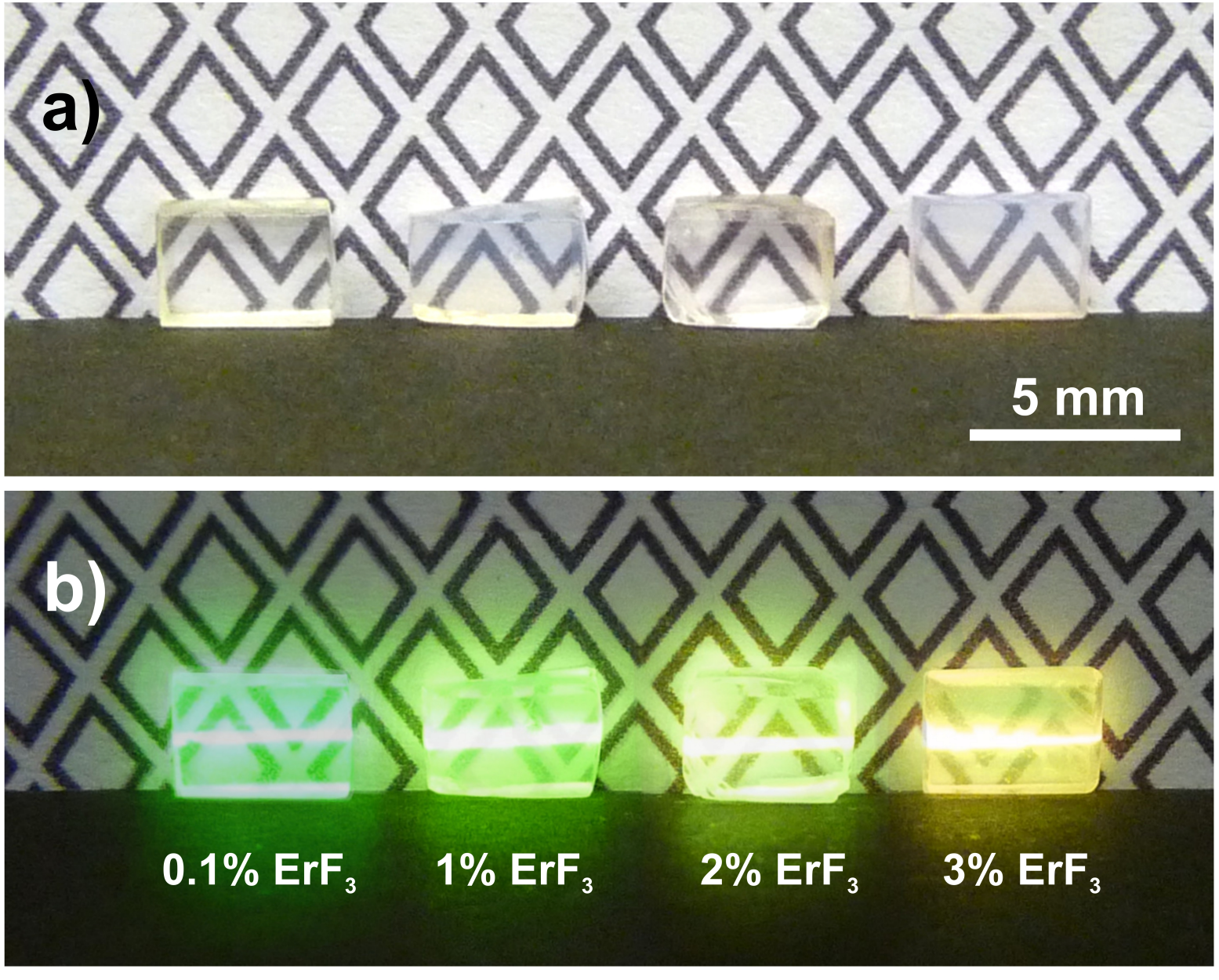
a)
5 mm
b)
0.1% ErF_3
1% ErF_3
2% ErF_3
3% ErF_3

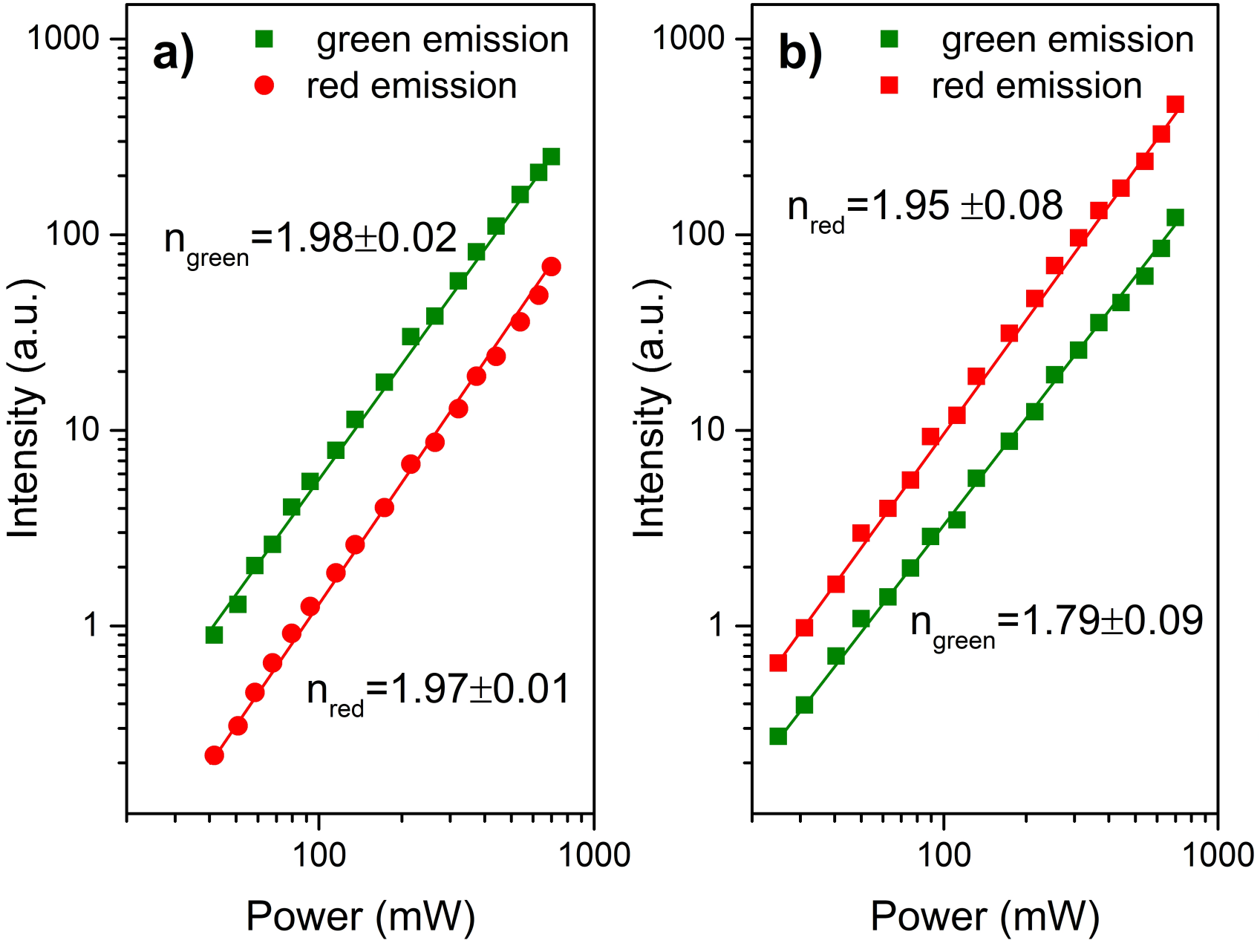
a)
green emission
red emission
n_{green}=1.98±0.02
n_{red}=1.97±0.01
Intensity (a.u.)
Power (mW)
1000
100
10
1
100
1000
b)
green emission
red emission
n_{red}=1.95 ±0.08
n_{green}=1.79±0.09
Intensity (a.u.)
Power (mW)
1000
100
10
1
100
1000

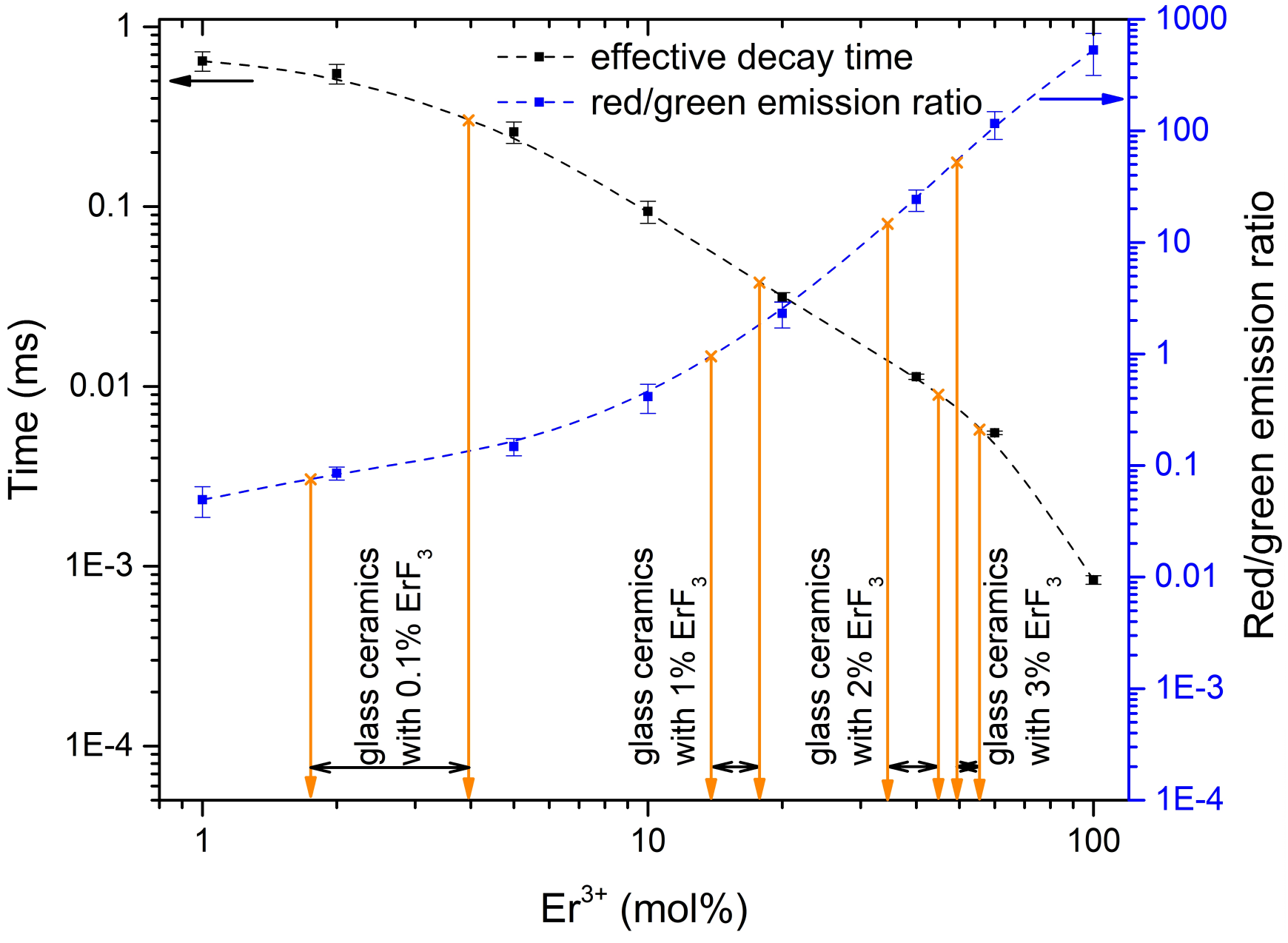
effective decay time
red/green emission ratio
Time (ms)
Red/green emission ratio
Er3+ (mol%)
1
0.1
0.01
1E-3
1E-4
1000
100
10
1
0.1
0.01
1E-3
1E-4
1
10
100
glass ceramics with 0.1% ErF3
glass ceramics with 1% ErF3
glass ceramics with 2% ErF3
glass ceramics with 3% ErF3

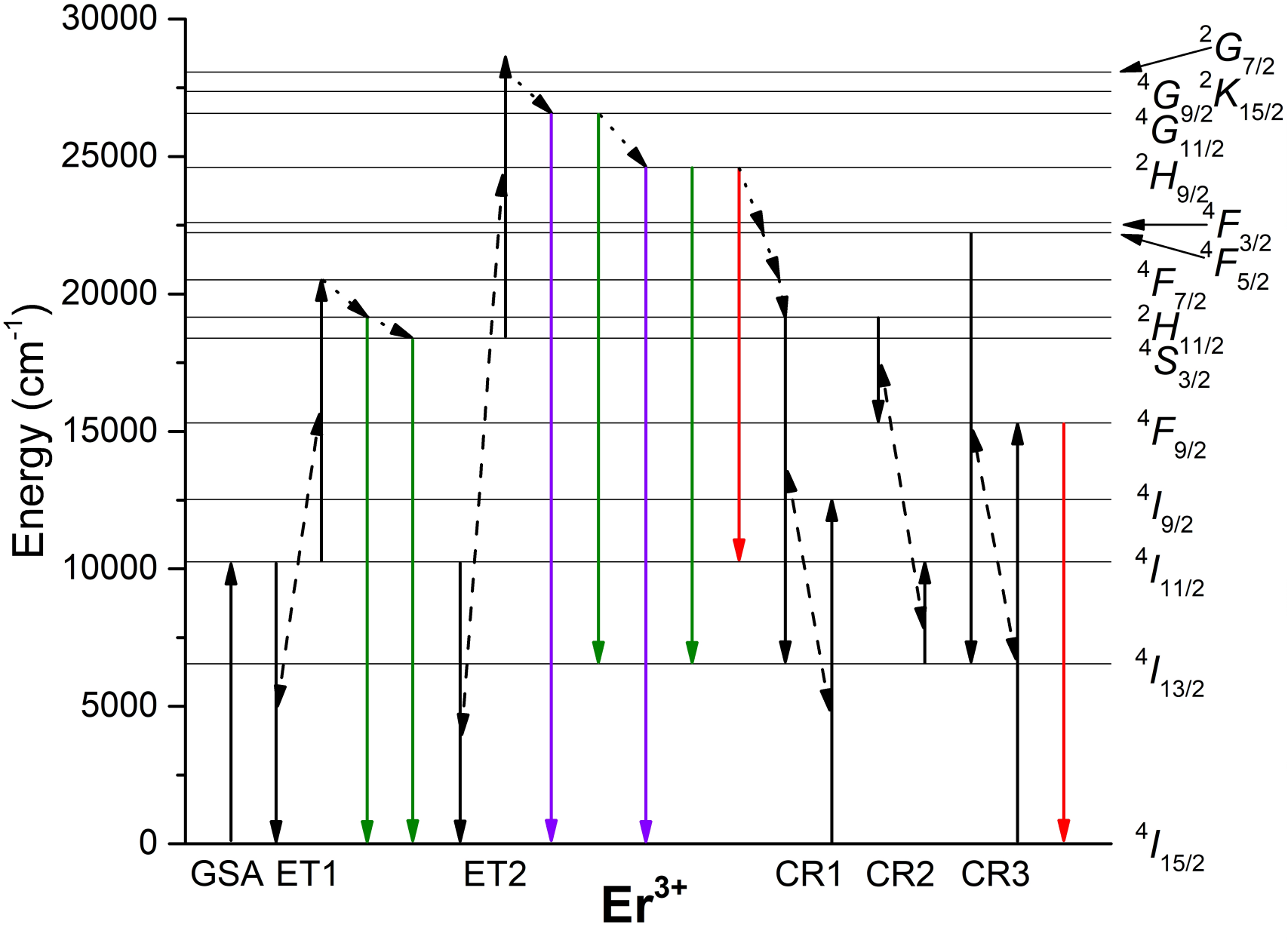
Energy (cm-1)
30000
25000
20000
15000
10000
5000
0
GSA
ET1
ET2
CR1
CR2
CR3
Er3+
2G7/2
4G9/2 2K15/2
4G11/2
2H9/2
4F3/2
4F5/2
4F7/2
2H11/2
4S3/2
4F9/2
4I9/2
4I11/2
4I13/2
4I15/2

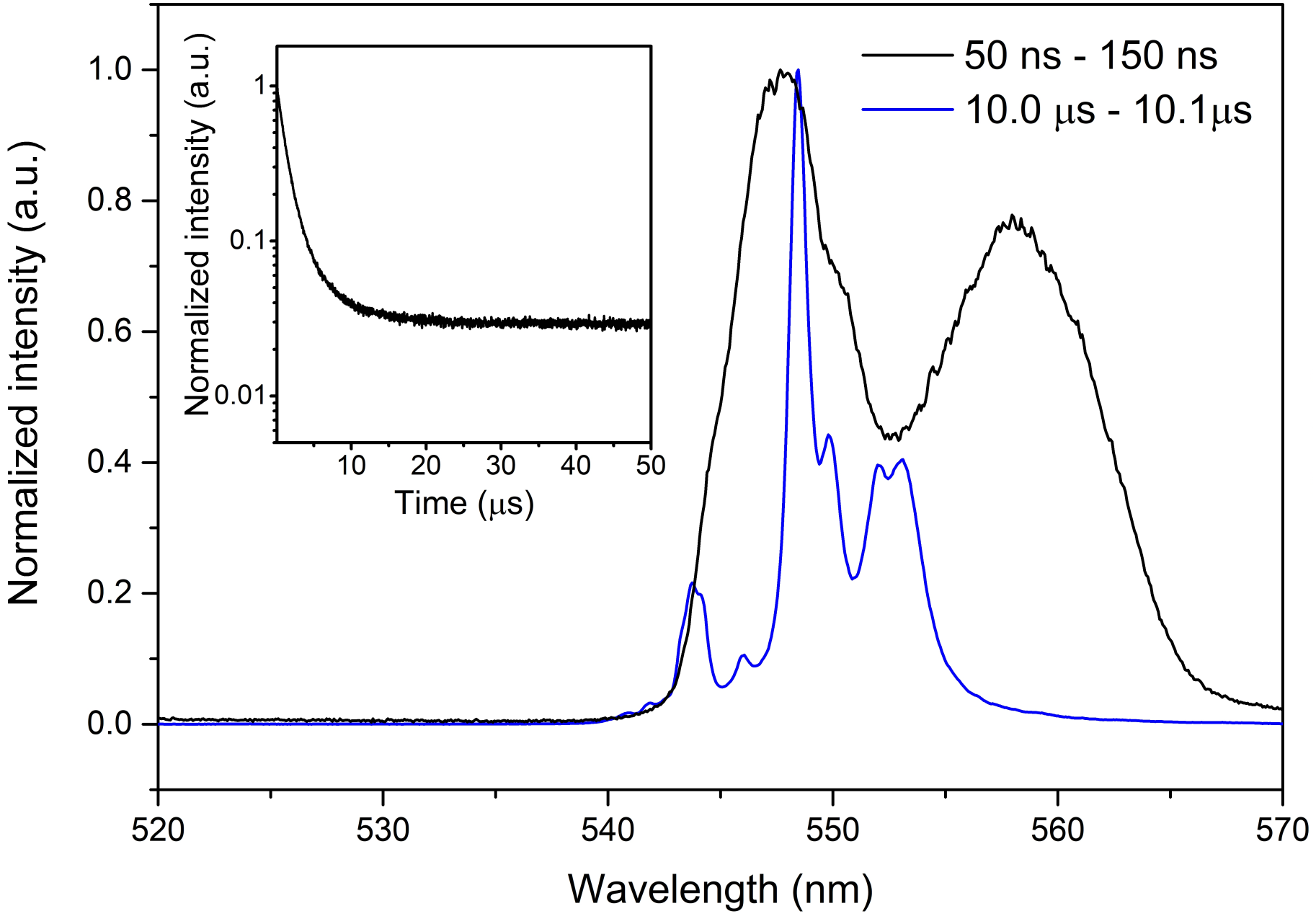
50 ns - 150 ns
10.0 μs - 10.1μs
Normalized intensity (a.u.)
Wavelength (nm)
Normalized intensity (a.u.)
Time (μs)

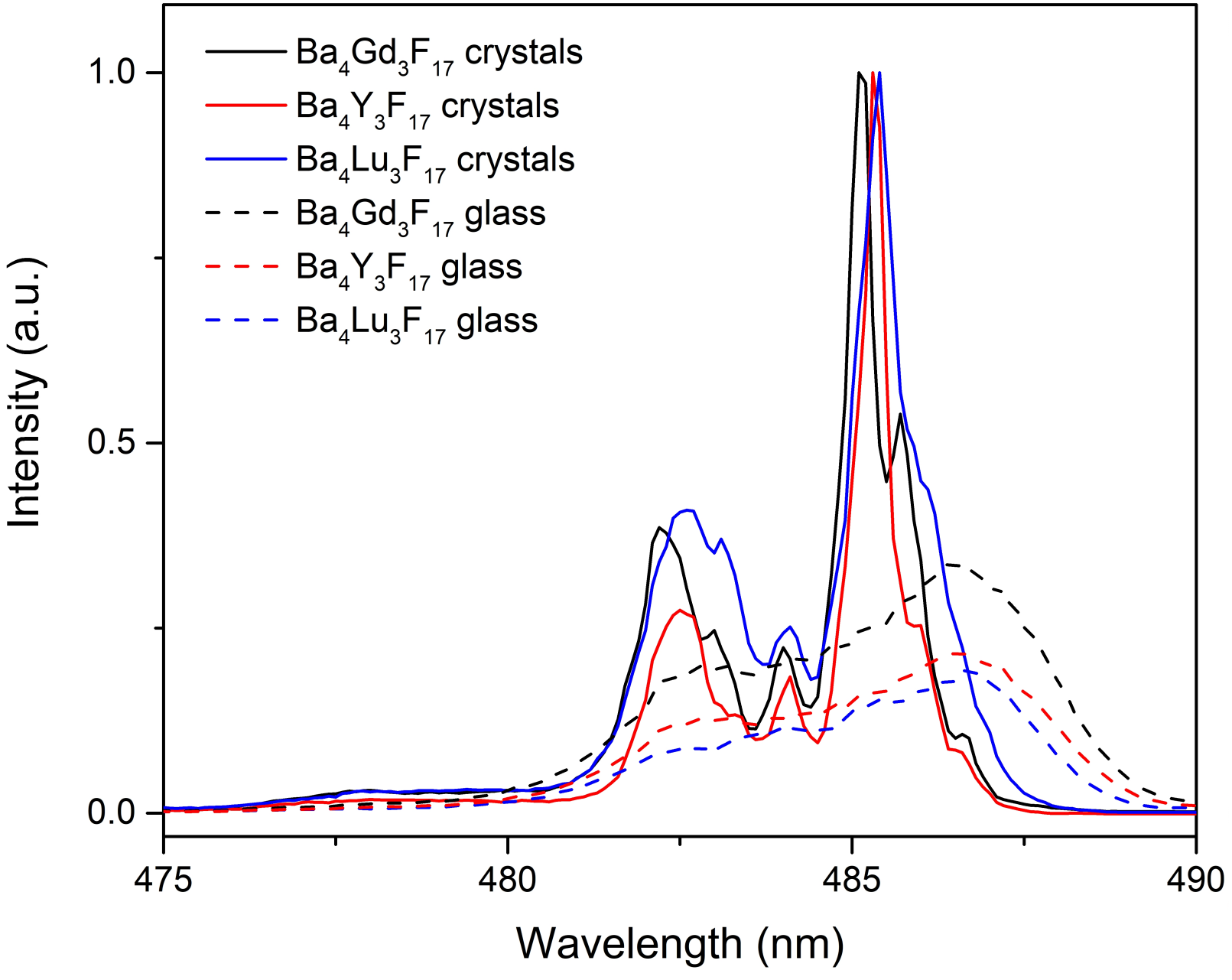
Ba4Gd3F17 crystals
Ba4Y3F17 crystals
Ba4Lu3F17 crystals
Ba4Gd3F17 glass
Ba4Y3F17 glass
Ba4Lu3F17 glass
Intensity (a.u.)
1.0
0.5
0.0
475
480
485
490
Wavelength (nm)

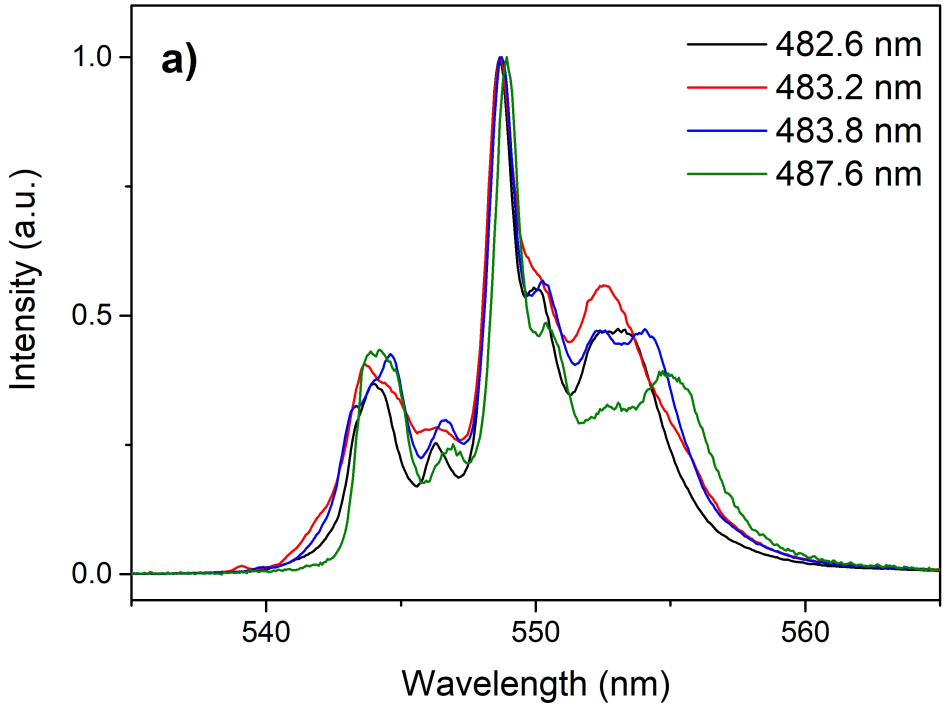
a)
482.6 nm
483.2 nm
483.8 nm
487.6 nm
Intensity (a.u.)
1.0
0.5
0.0
540
550
560
Wavelength (nm)

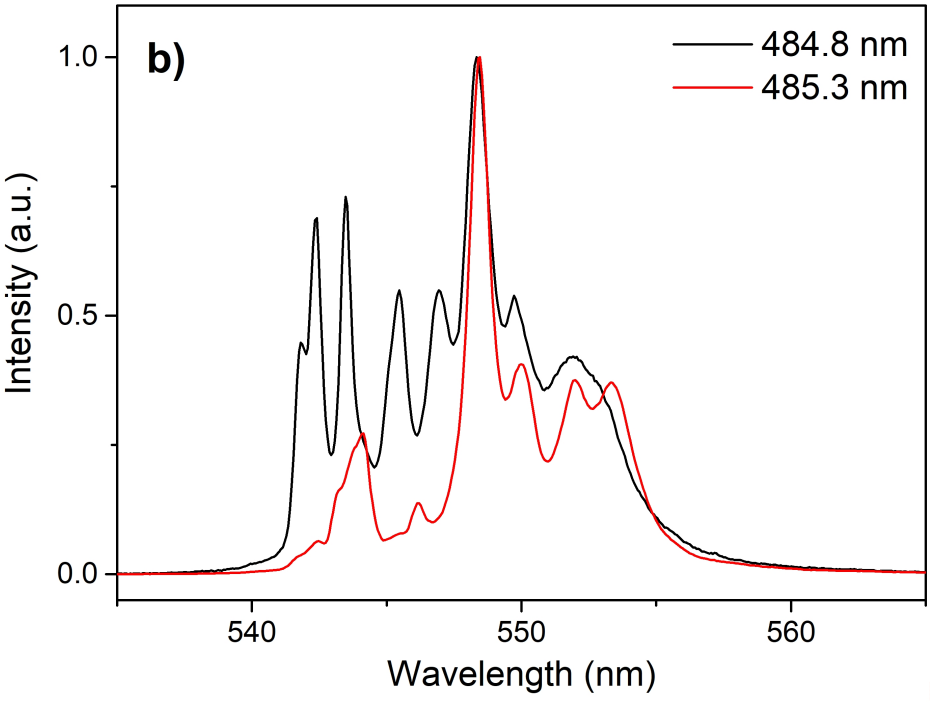
b)
484.8 nm
485.3 nm
Intensity (a.u.)
1.0
0.5
0.0
540
550
560
Wavelength (nm)

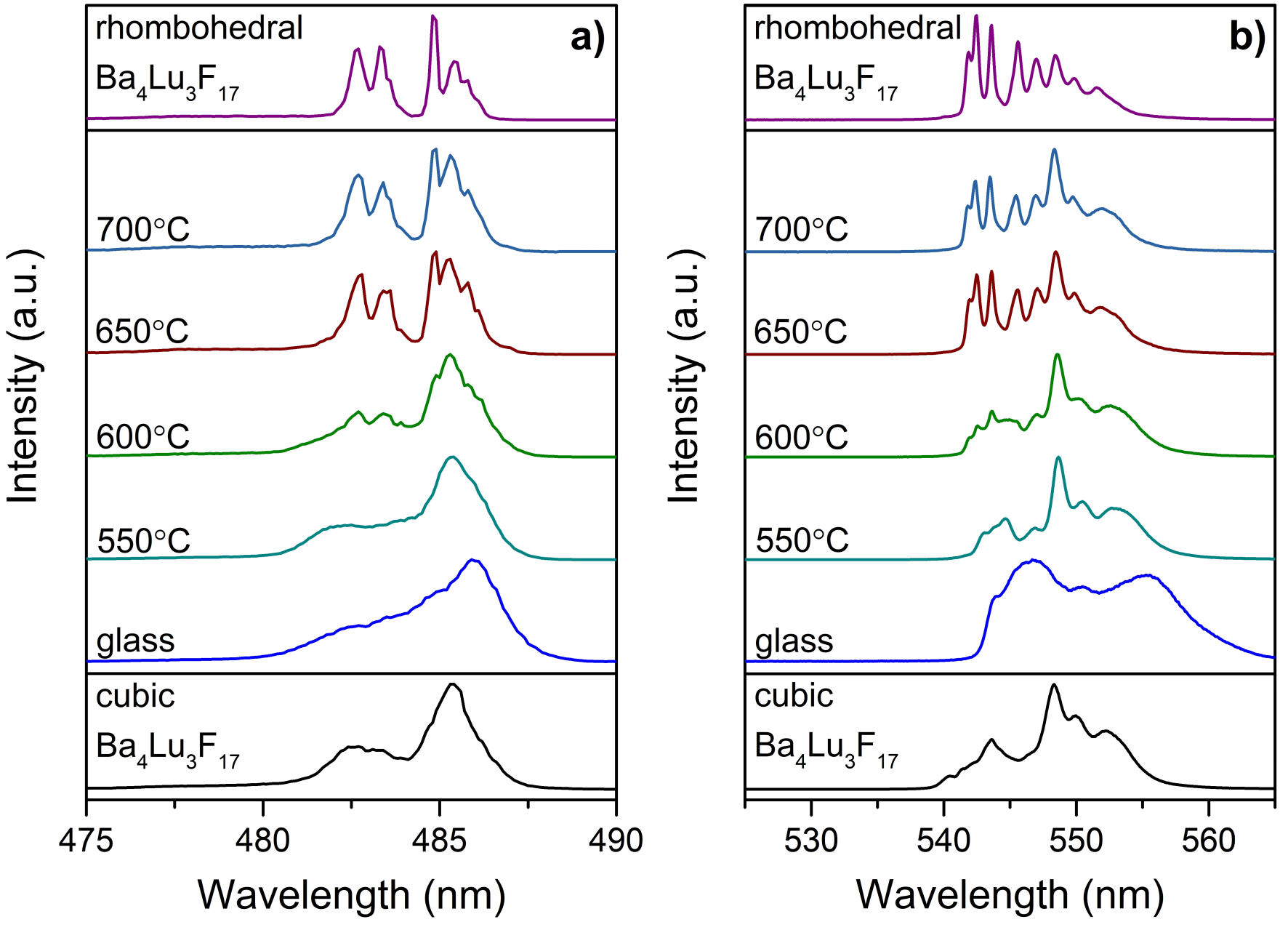
a)
rhombohedral
Ba4Lu3F17
700°C
650°C
600°C
550°C
glass
cubic
Ba4Lu3F17
Intensity (a.u.)
475
480
485
490
Wavelength (nm)
b)
rhombohedral
Ba4Lu3F17
700°C
650°C
600°C
550°C
glass
cubic
Ba4Lu3F17
Intensity (a.u.)
530
540
550
560
Wavelength (nm)